

## Responses to Comments of Referee #1

The authors have addressed my comments fully and clearly. I have a very minor point that came out while re-reading the manuscript and author responses.

In the response to my comment about the non-dimensionalization (my comment 6 -- covered on pages 3-4 of the author rebuttal document) the authors' mention they selected  $y_0$  as a characteristic length, but actually they used 2 characteristic lengths (they used  $H$  in the vertical direction). This leads to  $\kappa_z$  including not just the permeability ratio  $K_y/K_z$  (similar to  $\kappa_x$ ), but also the squared length scale ratio  $y_0^2/H^2$ . Because of this choice, one cannot disentangle the effects of changing  $\kappa_z$  that are due to permeability changes, or due to the square root of length scaling changes.

I understand it is too late in the process to change this sort of detail (and it does not change the results or impact of the manuscript), but a consistent single characteristic length scale would have been a bit simpler.

Response: Thanks for the comment. The definition of  $\kappa_z = K_z y_0^2 / (K_y H^2)$  can explicitly demonstrate that both  $K_z/K_y$  and  $y_0^2/H^2$  are crucial factors in neglecting the effect of the vertical flow on stream filtration/depletion rate (SDR) (Huang et al., 2014). Such definition is similar to the work of Neuman (1975) in which he defined dimensionless parameter  $\beta = K_z r^2 / (K_r H^2)$  with  $K_r$  representing the hydraulic conductivity in the radial direction and  $r$  denoting a radial distance measured from a pumping well to an observation point. He used the parameter to examine the validity of neglecting the effect of the vertical flow on time-dependent drawdown at the observation point (see Figure 1 in Neuman, 1975).

In our definition, the effect of  $K_z/K_y$  on SDR can be clearly explored once the value of  $y_0$  is selected. On the other hand, the effect of  $y_0^2/H^2$  on SDR can also be assessed if the value of  $K_z/K_y$  is known.

### References

- Huang, C. S., Lin, W. S., and Yeh, H. D.: Stream filtration induced by pumping in a confined, unconfined or leaky aquifer bounded by two parallel streams or by a stream and an impervious stratum, *J. Hydrol.*, 513, 28–44, doi:10.1016/j.jhydrol.2014.03.039, 2014.
- Neuman, S. P.: Analysis of pumping test data from anisotropic unconfined aquifers considering delayed gravity response, *Water Resour. Res.*, 11, 329–342, 1975.

## Responses to Comments of Referee #2

### Analysis of three-dimensional groundwater flow toward a radial collector well in a finite-extent unconfined aquifer-second review

The authors have addressed most of my comments. In my original review, I mentioned that the stream function presented for the case of section 3.1 does not exist. The answer of the authors to my objection is unsatisfactory. I understand from the problem description that the well is placed along  $z = 0.5$ ,  $9.5 \leq x \leq 10.5$ ,  $y = 1$ , while the for domain has width  $W_y = 20$ . This implies that the flow is three-dimensional. Although the authors present the flow net for  $y = 1$  and claim that the flow in  $y = 0$  is two-dimensional, this does not imply that the stream function exists. The presence of non-zero second order derivatives prevents the stream function, as presented by the authors, from being single-valued. Response: Thanks for the valuable comment on the fact that the stream function does not exist for three-dimensional flow. We realize that the stream function exists only for a few cases. For the cases of no stream function, one should rely on numerical approaches to determine the flow path lines. The path lines can be regarded as the streamlines for steady flow but not for transient flow.

We have removed the text associated with the stream function from section 3.1. The appendix C showing the derivation of the stream function is also removed. The section 3.1 is now slightly revised as:

#### “3.1 Identification of 3-D or 2-D flow at observation point

Most existing models assume 2-D flow with neglecting the vertical flow for pumping at a horizontal well (e.g., Mohamed and Rushton, 2006; Haitjema et al., 2010). The head distributions predicted by those models are inaccurate if an observation point is close to the region where the vertical flow prevails. Figure 2 demonstrates the equipotential lines predicted by the present solution for a horizontal well in an unconfined aquifer for  $\bar{x}_0 = 10$ ,  $\bar{w}_x = \bar{w}_y = 20$  and  $\kappa_z = 0.1, 1$ , and  $10$ . The well is located at  $9.5 \leq \bar{x} \leq 10.5$ ,  $\bar{y} = 1$  and  $\bar{z} = 0.5$  as illustrated in the figure. The equipotential lines are based on steady-state head distributions plotted by Eq. (44) with  $\bar{y} = 1$  and  $\bar{t} = 10^7$ . When  $\kappa_z = 0.1$ , in the range of  $10 \leq \bar{x} \leq 13.66$ , the contours of the hydraulic head are in a curved path, and the flow toward the well is thus slanted. Moreover, the range decreases to  $10 \leq \bar{x} \leq 11.5$  when  $\kappa_z = 1$  and to  $10 \leq \bar{x} \leq 10.82$  when  $\kappa_z = 10$ . Beyond these ranges, the head contours are nearly vertical, and the flow is essentially horizontal. Define  $\bar{d} = d/y_0$  as a shortest dimensionless horizontal distance between the well and a nearest location of only horizontal flow. The  $\bar{d}$  is therefore chosen as 3.16, 1 and 0.32 for the cases of  $\kappa_z = 0.1, 1$  and  $10$ , respectively. Substituting  $(\kappa_z, \bar{d}) = (0.1, 3.16), (1, 1)$  and  $(10, 0.32)$  into  $\kappa_z \bar{d}^2$  leads to about unity. We may therefore conclude that the vertical flow at an observation point is negligible if its location is beyond the range of  $\bar{d} < \sqrt{1/\kappa_z}$  (i.e.,  $d < H\sqrt{K_y/K_z}$ ) for thin aquifers, an observation point far from the well, and/or a small ratio of  $K_y/K_z$ .”

As a second comment, I remain of the opinion that the the paper would much benefit from a more

thorough validation, especially in view of my preceding statement. The comparison with Hunt's solution is given, but holds only for a very limited case.

Response: Please refer to the first response to the statement. The results in Figures 2–6 are plotted on the basis of the same computer program but with different parameters. We achieve agreement on stream depletion rate (SDR) predicted by the present solution and Hunt (1999) solution when adjusting parameters for the situation used to develop the latter solution. This indicates that the program and the derivation of the present solution are correct. In addition, Huang et al. (2012) verified their solution in comparison with the Hantush and Papadopoulos (1962) solution describing short-time and long-time drawdown distributions due to a radial collector well. The solution of Huang et al. (2012) is a special case of the present solution as discussed in section 2.6.4 of the revised manuscript. We would not repeat it in this revised manuscript; it has been discussed in detail in Huang et al. (2012).

## Summary

In my view, the use of the stream function in example 3.1 is in error. If I misunderstood their example as being three-dimensional, whereas in reality is two-dimensional, then the authors have to make this much more clear than in the present form of the paper. If the problem is indeed three-dimensional, then the use of the stream function must be removed from the paper. The reader may easily verify the truth of my statement by considering the case of a point sink at the origin in three-dimensional space. The discharge potential for that case has the form

$$\Phi = -\frac{Q}{4\pi} \frac{1}{r} \quad (1)$$

where

$$r^2 = x_1^2 + x_2^2 + x_3^2 \quad (2)$$

where  $x_i$ ,  $i = 1, 2, 3$ , are the Cartesian coordinates. Set  $x_3 = 0$ . Then

$$\Phi = \frac{Q}{4\pi} \frac{1}{\sqrt{x_1^2 + x_2^2}} \quad (3)$$

Introduce complex variables  $z = x_1 + iy_1$ ,  $\bar{z} = x_1 - iy_1$ , so that (3) becomes

$$\Phi = -\frac{Q}{4\pi} \frac{1}{\sqrt{z\bar{z}}} \quad (4)$$

This function is not holomorphic, and thus the stream function does not exist for this case.

Response: We appreciate reviewer's explanation in detail. The text associated with the stream function has been removed.

## References

Haitjema, H., Kuzin, S., Kelson, V., and Abrams, D.: Modeling flow into horizontal wells in a Dupuit-Forchheimer model, *Ground Water*, 48(6), 878–883, doi:10.1111/j.1745-

6584.2010.00694.x, 2010.

Hantush, M. S. and Papadopoulos, I. S.: Flow of groundwater to collector wells, J. Hydr. Eng. Div., 88(5), 221–244, 1962.

Huang, C. S., Tsou, P. R., and Yeh, H. D.: An analytical solution for a radial collector well near a stream with a low-permeability streambed, J. Hydrol., 446, 48–58, doi:10.1016/j.jhydrol.2012.04.028, 2012.

Hunt, B.: Unsteady stream depletion from ground water pumping, Ground Water, 37(1), 98–102, doi:10.1111/j.1745-6584.1999.tb00962.x, 1999.

Mohamed, A. and Rushton, K.: Horizontal wells in shallow aquifers: Field experiment and numerical model, J. Hydrol., 329(1–2), 98–109, doi:10.1016/j.jhydrol.2006.02.006, 2006.

**Figure**

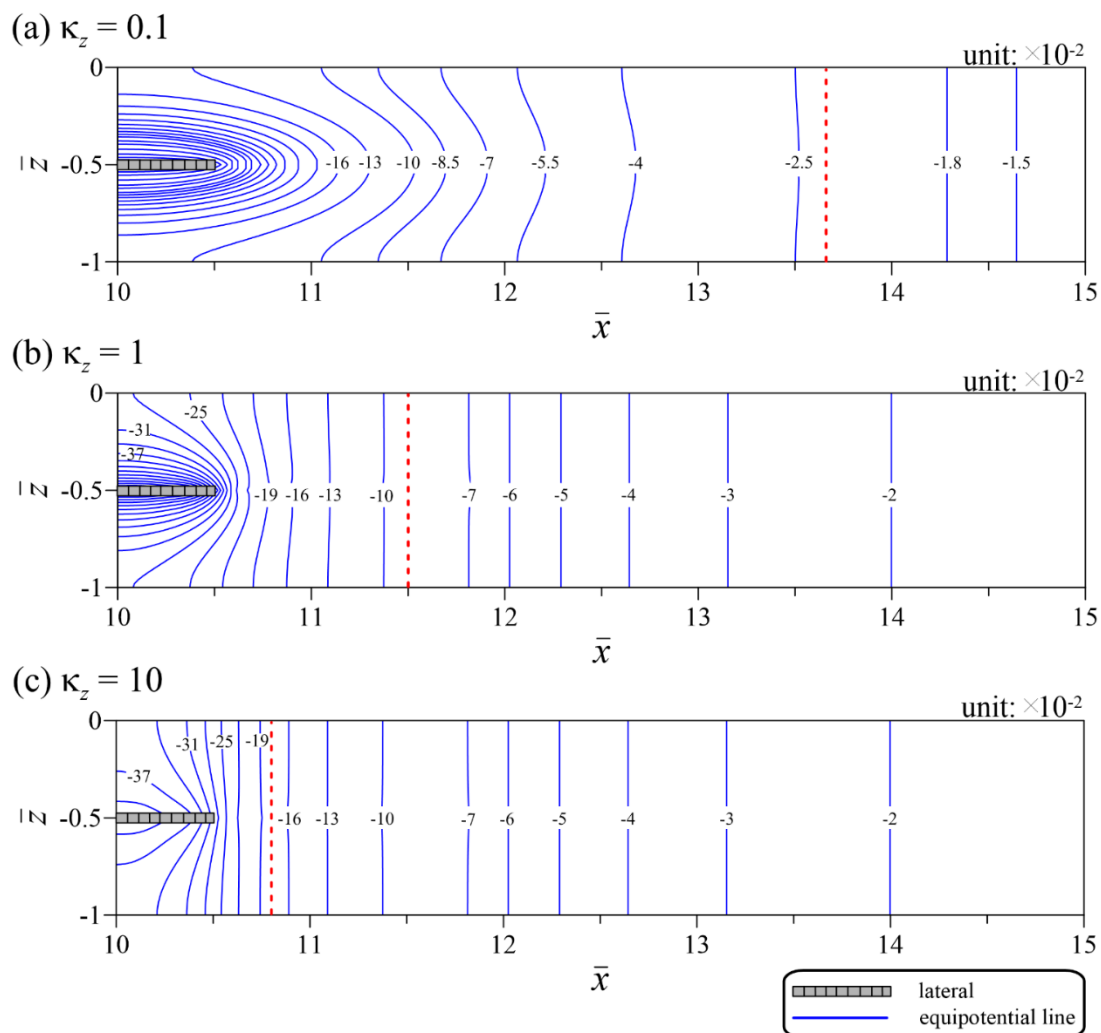


**Figure 2.** Equipotential lines predicted by the present solution for  $\kappa_z =$  (a) 0.1, (b) 1 and (c) 10.

1     **Approximate analysis of three-dimensional groundwater flow toward a**  
2             **radial collector well in a finite-extent unconfined aquifer**

3             **Ching-Sheng Huang<sup>1</sup>, Jyun-Jie Chen<sup>1</sup>, and Hund-Der Yeh<sup>1\*</sup>**

4  
5  
6  
7

8     **Submitted to *Hydrology and Earth System Sciences* on June 14, 2015**

9     **Re-submitted to *Hydrology and Earth System Sciences* on July 22, 2015**

10    **Re-re-submitted to *Hydrology and Earth System Sciences* on October 14, 2015**

11    **Re-re-re-submitted to *Hydrology and Earth System Sciences* on December 18, 2015**

12

13    <sup>1</sup> Institute of Environmental Engineering, National Chiao Tung University, Hsinchu, Taiwan.

14

15    **\* Corresponding Author**

16    Address: Institute of Environmental Engineering, National Chiao Tung University, 1001

17    University Road, Hsinchu 300, Taiwan

18    E-mail address: hdyeh@mail.nctu.edu.tw; Tel: 886-3-5731910; Fax: 886-3-5725958

19 **Abstract**

20 This study develops a three-dimensional mathematical model for describing transient  
21 hydraulic head distributions due to pumping at a radial collector well (RCW) in a rectangular  
22 confined or unconfined aquifer bounded by two parallel streams and no-flow boundaries. The  
23 streams with low-permeability streambeds fully penetrate the aquifer ~~thickness~~. The governing  
24 equation with a point-sink term is employed. A first-order free surface equation delineating the  
25 water table decline induced by the well is considered. Robin boundary conditions are adopted  
26 to describe fluxes across the streambeds. The head solution for the point sink is derived by  
27 applying the methods of finite integral transform and Laplace transform. The head solution for  
28 a RCW is obtained by integrating the point-sink solution along the laterals of the RCW and  
29 then dividing the integration result by the sum of lateral lengths. On the basis of Darcy's law  
30 and head distributions along the streams, the solution for the stream depletion rate (SDR) can  
31 also be developed. With the aid of the head and SDR solutions, the sensitivity analysis can then  
32 be performed to explore the response of the hydraulic head to the change in a specific parameter  
33 such as the horizontal and vertical hydraulic conductivities, streambed permeability, specific  
34 storage, specific yield, lateral length and well depth. Spatial head distributions subject to the  
35 anisotropy of aquifer hydraulic conductivities are analyzed. A quantitative criterion is provided  
36 to identify whether groundwater flow at a specific region is 3-D or 2-D without the vertical  
37 component. In addition, another criterion is also given to allow the neglect of vertical flow  
38 effect on SDR. Conventional 2-D flow models can be used to provide accurate head and SDR  
39 predictions if satisfying these two criteria.

40 **Keywords:** Robin boundary condition, sensitivity analysis, stream depletion rate, first-order  
41 free surface equation, analytical solution

42 **1. Introduction**

43 The applications of a radial collector well (RCW) have received much attention in the  
44 aspects of water resource supply and groundwater remediation since rapid advances in drilling  
45 technology. An average yield for the well approximates 27,000 m<sup>3</sup>/day (Todd and Mays, 2005).  
46 As compared to vertical wells, RCWs require less operating cost, produce smaller drawdown,  
47 and have better efficiency of withdrawing water from thin aquifers. In addition, RCWs can  
48 extract water from an aquifer underlying obstacles such as buildings, but vertical wells cannot.  
49 Recently, Huang et al. (2012) reviewed semi-analytical and analytical solutions associated with  
50 RCWs. Since then, Yeh and Chang (2013) provided a valuable overview of articles associated  
51 with RCWs.

52 A variety of analytical models involving a horizontal well, a specific case of a RCW with  
53 a single lateral, in aquifers were developed (e.g., Park and Zhan, 2003; Hunt, 2005; Anderson,  
54 2013). The flux along the well screen is commonly assumed to be uniform. The equation  
55 describing three-dimensional (3-D) flow is used. Kawecki (2000) developed analytical  
56 solutions of the hydraulic heads for the early linear flow perpendicular to a horizontal well and  
57 late pseudo-radial flow toward the middle of the well in confined aquifers. They also developed  
58 an approximate solution for unconfined aquifers on the basis of the head solution and an  
59 unconfined flow modification. The applicability of the approximate solution was later  
60 evaluated in comparison with a finite difference solution developed by Kawecki and Al-  
61 Subaikhy (2005). Zhan et al. (2001) presented an analytical solution for drawdown induced by  
62 a horizontal well in confined aquifers and compared the difference in the type curves based on  
63 the well and a vertical well. Zhan and Zlotnik (2002) developed a semi-analytical solution of  
64 drawdown due to pumping from a nonvertical well in an unconfined aquifer accounting for the  
65 effect of instantaneous drainage or delayed yield when the free surface declines. They discussed  
66 the influences of the length, depth, and inclination of the well on temporal drawdown

67 distributions. Park and Zhan (2002) developed a semi-analytical drawdown solution  
68 considering the effects of a finite diameter, the wellbore storage, and a skin zone around a  
69 horizontal well in anisotropic leaky aquifers. They found that those effects cause significant  
70 change in drawdown at an early pumping period. Zhan and Park (2003) provided a general  
71 semi-analytical solution for pumping-induced drawdown in a confined aquifer, an unconfined  
72 aquifer on a leaky bottom, or a leaky aquifer below a water reservoir. Temporal drawdown  
73 distributions subject to the aquitard storage effect were compared with those without that effect.  
74 Sun and Zhan (2006) derived a semi-analytical solution of drawdown due to pumping at a  
75 horizontal well in a leaky aquifer. A transient one-dimensional flow equation describing the  
76 vertical flow across the aquitard was considered. The derived solution was used to evaluate the  
77 Zhan and Park (2003) solution which assumed steady-state vertical flow in the aquitard.

78       Sophisticated numerical models involved in RCWs or horizontal wells were also reported.  
79 Steward (1999) applied the analytic element method to approximate 3-D steady-state flow  
80 induced by horizontal wells in contaminated aquifers. They discussed the relation between a  
81 pumping rate and the size of a polluted area. Chen et al. (2003) utilized the polygon finite  
82 difference method to deal with three kinds of seepage-pipe flows including laminar, turbulent,  
83 and transitional flows within a finite-diameter horizontal well. A sandbox experiment was also  
84 carried out to verify the prediction made by the method. Mohamad and Rushton (2006) used  
85 MODFLOW to predict flows inside an aquifer, from the aquifer to a horizontal well, and within  
86 the well. The predicted head distributions were compared with field data measured in Sarawak,  
87 Malaysia. Su et al. (2007) used software TOUGH2 based on the integrated finite difference  
88 method to handle irregular configurations of several laterals of two RCWs installed beside the  
89 Russian River, Forestville, California and analyzed pumping-induced unsaturated regions  
90 beneath the river. Lee et al. (2012) developed a finite element solution with triangle elements  
91 to assess whether the operation of a RCW near Nakdong River in South Korea can induce



92 riverbank filtration. They concluded that the well can be used for sustainable water supply at  
93 the study site. In addition, Rushton and Brassington (2013a) extended Mohamad and Rushton  
94 (2006) study by enhancing the Darcy-Weisbach formula to describe frictional head loss inside  
95 a horizontal well. The spatial distributions of predicted flux along the well revealed that the  
96 flux at the pumping end is four times of the magnitude of that at the far end. Later, Rushton  
97 and Brassington (2013b) applied the same model to a field experiment at the Seton Coast,  
98 northwest England.

99 Well pumping in aquifers near streams may cause groundwater–surface water interactions  
100 (e.g., Rodriguez et al., 2013; Chen et al., 2013; Zhou et al., 2013; Exner-Kittridge et al., 2014;  
101 Flipo et al., 2014; Unland et al., 2014). The stream depletion rate (SDR), commonly used to  
102 quantify stream water filtration into the adjacent aquifer, is defined as the ratio of the filtration  
103 rate to a pumping rate. The SDR ranges from zero to a certain value which could be equal to  
104 or less than unity (Zlotnik, 2004). Tsou et al. (2010) developed an analytical solution of SDR  
105 for a slanted well in confined aquifers adjacent to a stream treated as a constant-head boundary.  
106 They indicated that a horizontal well parallel to the stream induces the steady-state SDR of  
107 unity more quickly than a slanted well. Huang et al. (2011) developed an analytical SDR  
108 solution for a horizontal well in unconfined aquifers near a stream regarded as a constant-head  
109 boundary. Huang et al. (2012) provided an analytical solution for SDR induced by a RCW in  
110 unconfined aquifers adjacent to a stream with a low-permeability streambed ~~treated as under~~  
111 the Robin condition. The influence of the configuration of the laterals on temporal SDR and  
112 spatial drawdown distributions was analyzed. Recently, Huang et al. (2014) gave an exhaustive  
113 review on analytical and semi-analytical SDR solutions and classified these solutions into two  
114 categories. One group involved two-dimensional (2-D) flow toward a fully-penetrating vertical  
115 well according to aquifer types and stream treatments. The other group included the solutions  
116 involving 3-D and quasi 3-D flows in the lights of aquifer types, well types, and stream

117 treatments.

118 At present, existing analytical solutions associated with flow toward a RCW in unconfined  
119 aquifers have involved laborious calculation (Huang et al., 2012) and predicted approximate  
120 results (Hantush and Papadopoulos, 1962). The Huang et al. (2012) solution involves numerical  
121 integration of a triple integral in predicting the hydraulic head and a quintuple integral in  
122 predicting SDR. The integrand is expressed in terms of an infinite series expanded by roots of  
123 nonlinear equations. The integration variables are related to those roots. The application of  
124 their solution is therefore limited to those who are familiar with numerical methods. In addition,  
125 the accuracy of the Hantush and Papadopoulos (1962) solution is limited to some parts of a  
126 pumping period; that is, it gives accurate drawdown predictions at early and late times but  
127 divergent ones at middle time.

128 The objective of this study is to present new analytical solutions of the head and SDR,  
129 which overcome the above-mentioned limitations, for 3-D flow toward a RCW. A  
130 mathematical model is built to describe 3-D spatiotemporal hydraulic head distributions in a  
131 rectangular unconfined aquifer bounded by two parallel streams and by the no-flow stratum  
132 in the other two sides. The flux across the well screen is assumed to be uniform along each of  
133 the laterals. The assumption is valid for a short lateral within 150 m verified by agreement on  
134 drawdown observed in field experiments and predicted by existing analytical solutions (Huang  
135 et al., 2011; 2012). The streams fully penetrate the aquifer ~~thickness~~ and connect the aquifer  
136 with low-permeability streambeds. The model for the aquifer system with two parallel streams  
137 can be used to determine the fraction of water filtration from the streams and solve the  
138 associated water right problem (Sun and Zhan, 2007). The transient 3-D groundwater flow  
139 equation with a point-sink term is considered. The first-order free surface equation is used to  
140 describe water table decline due to pumping. Robin boundary conditions are adopted to  
141 describe fluxes across the streambeds. The head solution for a point sink is derived by the

142 methods of Laplace transform and finite integral transform. The analytical head solution for a  
143 RCW is then obtained by integrating the point-sink solution along the well and dividing the  
144 integration result by the total lateral length. The RCW head solution is expressed in terms of a  
145 triple series expanded by eigenvalues which can be obtained by a numerical algorithm such as  
146 Newton's method. On the basis of Darcy's law and the RCW head solution, the SDR solution  
147 can then be obtained in terms of a double series with fast convergence. With the aid of both  
148 solutions, the sensitivity analysis is performed to investigate the response of the hydraulic head  
149 to the change in each of aquifer parameters. ~~The spatial distributions of the head and streamline~~  
150 ~~are discussed.~~ Spatial head distributions subject to the anisotropy of aquifer hydraulic  
151 conductivities are analyzed. The influences of the vertical flow and well depth on temporal  
152 SDR distributions are investigated. Moreover, temporal SDR distributions induced by a RCW  
153 and a fully penetrating vertical well in confined aquifers are also compared. A quantitative  
154 criterion is provided to identify whether groundwater flow at a specific region is 3-D or 2-D  
155 without the vertical component. In addition, another criterion is also given to judge the  
156 suitability of neglecting the vertical flow effect on SDR.

157

## 158 **2. Methodology**

### 159 **2.1. Mathematical model**

160 Consider a RCW in a rectangular unconfined aquifer bounded by two parallel streams and  
161 no-flow stratum as illustrated in Figure 1. The symbols for variables and parameters are  
162 defined in Table 1. The origin of the Cartesian coordinate is located at the lower left corner.  
163 The aquifer domain falls in the range of  $0 \leq x \leq w_x$ ,  $0 \leq y \leq w_y$ , and  $-H \leq z \leq 0$ . The  
164 RCW consists of a caisson and several laterals, each of which extends ~~finitely~~ with length  $L_k$   
165 and counterclockwise with angle  $\theta_k$  where  $k \in 1, 2, \dots, N$  and  $N$  is the number of laterals. The  
166 caisson is located at  $(x_0, y_0)$ , and the surrounding laterals are at  $z = -z_0$ .

167 First of all, a mathematical model describing 3-D flow toward a point sink in the aquifer  
 168 is proposed. The equation describing 3-D hydraulic head distribution  $h(x, y, z, t)$  is expressed  
 169 as

$$170 \quad K_x \frac{\partial^2 h}{\partial x^2} + K_y \frac{\partial^2 h}{\partial y^2} + K_z \frac{\partial^2 h}{\partial z^2} = S_s \frac{\partial h}{\partial t} + Q \delta(x - x'_0) \delta(y - y'_0) \delta(z + z'_0) \quad (1)$$

171 where  $\delta(\ )$  is the Dirac delta function, the second term on the right-hand side (RHS) indicates  
 172 the point sink, and  $Q$  is positive for pumping and negative for injection. The first term on the  
 173 RHS of Eq. (1) depicts aquifer storage release based on the concept of effective stress proposed  
 174 by Terzaghi (see, for example, Bear, 1979; Charbeneau, 2000), which is valid under the  
 175 assumption of constant total stress. By choosing water table as a reference datum where the  
 176 elevation head is set to zero, the initial condition can therefore be denoted as

$$177 \quad h = 0 \quad \text{at} \quad t = 0 \quad (2)$$

178 Note that equation (2) introduces negative hydraulic head for pumping, and the absolute value  
 179 of the head equals drawdown.

180 The aquifer boundaries at  $x = 0$  and  $x = w_x$  are considered to be impermeable and thus  
 181 expressed as

$$182 \quad \partial h / \partial x = 0 \quad \text{at} \quad x = 0 \quad (3)$$

183 and

$$184 \quad \partial h / \partial x = 0 \quad \text{at} \quad x = w_x \quad (4)$$

185 Streambed permeability is usually less than the adjacent aquifer formation. The fluxes across  
 186 the streambeds can be described by Robin boundary conditions as

$$187 \quad K_y \frac{\partial h}{\partial y} - \frac{K_1}{b_1} h = 0 \quad \text{at} \quad y = 0 \quad (5)$$

188 and

$$189 \quad K_y \frac{\partial h}{\partial y} + \frac{K_2}{b_2} h = 0 \quad \text{at} \quad y = w_y \quad (6)$$

190 The free surface equation describing water table decline is written as

191 
$$K_x \left( \frac{\partial h}{\partial x} \right)^2 + K_y \left( \frac{\partial h}{\partial y} \right)^2 + K_z \left( \frac{\partial h}{\partial z} \right)^2 - K_z \frac{\partial h}{\partial z} = S_y \frac{\partial h}{\partial t} \quad \text{at } z = h \quad (7)$$

192 Neuman (1972) indicated that the effect of the second-order terms in Eq. (7) is generally  
193 ignorable to develop analytical solutions. Eq. (7) is thus linearized by neglecting the quadratic  
194 terms, and the position of the water table is fixed at the initial condition (i.e.,  $z = 0$ ). The result  
195 is written as

196 
$$K_z \frac{\partial h}{\partial z} = -S_y \frac{\partial h}{\partial t} \quad \text{at } z = 0 \quad (8)$$

197 Notice that Eq. (8) is applicable when the conditions  $|h|/H \leq 0.1$  and  $|\partial h / \partial x| +$   
198  $|\partial h / \partial y| \leq 0.01$  are satisfied. These two conditions had been studied and verified by  
199 simulations in, for example, Nyholm et al. (2002), Goldscheider and Drew (2007) and Yeh et  
200 al. (2010). Nyholm et al. (2002) achieved agreement on drawdown measured in a field pumping  
201 test and predicted by MODFLOW which models flow in the study site as confined behavior  
202 because of  $|h|/H \leq 0.1$  in the pumping well. Goldscheider and Drew (2007) revealed that  
203 pumping drawdown predicted by Neuman (1972) analytical solution based on Eq. (8) agrees  
204 well with that obtained in a field pumping test. In addition, Yeh et al. (2010) also achieved  
205 agreement on the hydraulic head predicted by their analytical solution based on Eq. (8), their  
206 finite difference solution based on Eq. (7) with  $\partial h / \partial y = 0$  (referring to Eq. (7a)), and Teo et  
207 al. (2003) solution derived by applying the perturbation technique to deal with Eq. (7a) when  
208  $|h|/H = 0.1$  and  $|\partial h / \partial x| = 0.01$  (i.e.,  $\alpha = 0.1$  and  $|\partial \phi / \partial x| = 0.01$  at  $x = 0$  in Yeh et al.  
209 (2010, Fig. 5(a)). On the other hand, the bottom of the aquifer is considered as a no-flow  
210 boundary condition denoted as

211 
$$\partial h / \partial z = 0 \quad \text{at } z = -H \quad (9)$$

212 Define dimensionless variables as  $\bar{h} = (K_y H h) / Q$ ,  $\bar{t} = (K_y t) / (S_y y_0^2)$ ,  $\bar{x} = x / y_0$ ,

213  $\bar{y} = y/y_0$ ,  $\bar{z} = z/H$ ,  $\bar{x}'_0 = x'_0/y_0$ ,  $\bar{y}'_0 = y'_0/y_0$ ,  $\bar{z}'_0 = z'_0/H$ ,  $\bar{w}_x = w_x/y_0$  and  $\bar{w}_y =$   
 214  $w_y/y_0$  where the overbar denotes a dimensionless symbol,  $H$  is the initial aquifer thickness,  
 215 and  $y_0$  is a distance between stream 1 and the center of the RCW, is chosen as a characteristic  
 216 length. On the basis of the definitions, Eq. (1) can be written as

$$217 \quad \kappa_x \frac{\partial^2 \bar{h}}{\partial \bar{x}^2} + \frac{\partial^2 \bar{h}}{\partial \bar{y}^2} + \kappa_z \frac{\partial^2 \bar{h}}{\partial \bar{z}^2} = \frac{\partial \bar{h}}{\partial \bar{t}} + \delta(\bar{x} - \bar{x}'_0) \delta(\bar{y} - \bar{y}'_0) \delta(\bar{z} + \bar{z}'_0) \quad (10)$$

218 where  $\kappa_x = K_x/K_y$  and  $\kappa_z = (K_z y_0^2)/(K_y H^2)$ .

219 Similarly, the initial and boundary conditions are expressed as

$$220 \quad \bar{h} = 0 \quad \text{at} \quad \bar{t} = 0 \quad (11)$$

$$221 \quad \partial \bar{h} / \partial \bar{x} = 0 \quad \text{at} \quad \bar{x} = 0 \quad (12)$$

$$222 \quad \partial \bar{h} / \partial \bar{x} = 0 \quad \text{at} \quad \bar{x} = \bar{w}_x \quad (13)$$

$$223 \quad \partial \bar{h} / \partial \bar{y} - \kappa_1 \bar{h} = 0 \quad \text{at} \quad \bar{y} = 0 \quad (14)$$

$$224 \quad \partial \bar{h} / \partial \bar{y} + \kappa_2 \bar{h} = 0 \quad \text{at} \quad \bar{y} = \bar{w}_y \quad (15)$$

$$225 \quad \frac{\partial \bar{h}}{\partial \bar{z}} = -\frac{\gamma}{\kappa_z} \frac{\partial \bar{h}}{\partial \bar{t}} \quad \text{at} \quad \bar{z} = 0 \quad (16)$$

226 and

$$227 \quad \partial \bar{h} / \partial \bar{z} = 0 \quad \text{at} \quad \bar{z} = -1 \quad (17)$$

228 where  $\kappa_1 = (K_1 y_0)/(K_y b_1)$ ,  $\kappa_2 = (K_2 y_0)/(K_y b_2)$  and  $\gamma = S_y/(S_s H)$ .

## 229 2.2 Head solution for point sink

230 The model, Eqs. (10) – (17), reduces to an ordinary differential equation (ODE) with two  
 231 boundary conditions in terms of  $\bar{z}$  after taking Laplace transform and finite integral transform.

232 The former transform converts  $\bar{h}(\bar{x}, \bar{y}, \bar{z}, \bar{t})$  into  $\hat{h}(\bar{x}, \bar{y}, \bar{z}, p)$ ,  $\delta(\bar{x} - \bar{x}'_0) \delta(\bar{y} - \bar{y}'_0) \delta(\bar{z} - \bar{z}'_0)$

233 in Eq. (10) into  $\delta(\bar{x} - \bar{x}'_0) \delta(\bar{y} - \bar{y}'_0) \delta(\bar{z} - \bar{z}'_0)/p$ , and  $\partial \bar{h} / \partial \bar{t}$  in Eqs. (10) and (16) into

234  $p \hat{h} - \bar{h}|_{\bar{t}=0}$  where  $p$  is the Laplace parameter, and the second term, initial condition in Eq. (11),

235 equals zero (Kreyszig, 1999). The transformed model becomes a boundary value problem  
 236 written as

$$237 \quad \kappa_x \frac{\partial^2 \hat{h}}{\partial \bar{x}^2} + \frac{\partial^2 \hat{h}}{\partial \bar{y}^2} + \kappa_z \frac{\partial^2 \hat{h}}{\partial \bar{z}^2} = p \hat{h} + \delta(\bar{x} - \bar{x}'_0) \delta(\bar{y}' - \bar{y}'_0) \delta(\bar{z} + \bar{z}'_0) / p \quad (18)$$

238 with boundary conditions  $\partial \hat{h} / \partial \bar{x} = 0$  at  $\bar{x} = 0$  and  $\bar{x} = \bar{w}_x$ ,  $\partial \hat{h} / \partial \bar{y} - \kappa_1 \hat{h} = 0$  at  $\bar{y} = 0$ ,  
 239  $\partial \hat{h} / \partial \bar{y} + \kappa_2 \hat{h} = 0$  at  $\bar{y} = \bar{w}_y$ ,  $\partial \hat{h} / \partial \bar{z} = -p \gamma \hat{h} / \kappa_z$  at  $\bar{z} = 0$  and  $\partial \hat{h} / \partial \bar{z} = 0$  at  $\bar{z} = -1$ .

240 We then apply finite integral transform to the problem. One can refer to Appendix A for its  
 241 detailed definition. The transform converts  $\hat{h}(\bar{x}, \bar{y}, \bar{z}, p)$  in the problem into  $\tilde{h}(\alpha_m, \beta_n, \bar{z}, p)$ ,  
 242 and  $\delta(\bar{x} - \bar{x}'_0) \delta(\bar{y} - \bar{y}'_0)$  in Eq. (18) into  $\cos(\alpha_m \bar{x}'_0) K(\bar{y}'_0)$  and  $\kappa_x \partial^2 \hat{h} / \partial \bar{x}^2 + \partial^2 \hat{h} / \partial \bar{y}^2$   
 243 in Eq. (18) into  $-(\kappa_x \alpha_m^2 + \beta_n^2) \tilde{h}$  where  $(m, n) \in 1, 2, 3, \dots, \infty$ ,  $\alpha_m = m \pi / \bar{w}_x$ ,  $K(\bar{y}'_0)$  is  
 244 defined in Eq. (A2) with  $\bar{y} = \bar{y}'_0$ , and  $\beta_n$  ~~are~~ represents eigenvalues equaling the roots of the  
 245 following equation as (Latinopoulos, 1985)

$$246 \quad \tan(\beta_n \bar{w}_y) = \frac{\beta_n (\kappa_1 + \kappa_2)}{\beta_n^2 - \kappa_1 \kappa_2} \quad (19)$$

247 The method to determine the roots is discussed in section 2.3. In turn, Eq. (18) becomes a  
 248 second-order ODE defined by

$$249 \quad \kappa_z \frac{\partial^2 \tilde{h}}{\partial \bar{z}^2} - (\kappa_x \alpha_m^2 + \beta_n^2 + p) \tilde{h} = \cos(\alpha_m \bar{x}'_0) K(\bar{y}'_0) \delta(\bar{z} + \bar{z}'_0) / p \quad (20)$$

250 with two boundary conditions denoted as

$$251 \quad \frac{\partial \tilde{h}}{\partial \bar{z}} = -\frac{p \gamma}{\kappa_z} \tilde{h} \quad \text{at} \quad \bar{z} = 0 \quad (21)$$

252 and

$$253 \quad \partial \tilde{h} / \partial \bar{z} = 0 \quad \text{at} \quad \bar{z} = -1 \quad (22)$$

254 Eq. (20) can be separated into two homogeneous ODEs as

$$255 \quad \kappa_z \frac{\partial^2 \tilde{h}_a}{\partial \bar{z}^2} - (\kappa_x \alpha_m^2 + \beta_n^2 + p) \tilde{h}_a = 0 \quad \text{for} \quad -\bar{z}'_0 \leq \bar{z} \leq 0 \quad (23)$$

256 and

$$257 \quad \kappa_z \frac{\partial^2 \tilde{h}_b}{\partial \bar{z}^2} - (\kappa_x \alpha_m^2 + \beta_n^2 + p) \tilde{h}_b = 0 \quad \text{for} \quad -1 \leq \bar{z} \leq -\bar{z}'_0 \quad (24)$$

258 where  $h_a$  and  $h_b$ , respectively, represent the heads above and below  $\bar{z} = -\bar{z}'_0$  where the point  
259 sink is located. Two continuity requirements should be imposed at  $\bar{z} = -\bar{z}'_0$ . The first is the  
260 continuity of the hydraulic head denoted as

$$261 \quad \tilde{h}_a = \tilde{h}_b \quad \text{at} \quad \bar{z} = -\bar{z}'_0 \quad (25)$$

262 The second describes the discontinuity of the flux due to point pumping represented by the  
263 Dirac delta function in Eq. (20). It can be derived by integrating Eq. (20) from  $\bar{z} = -\bar{z}'_0^-$  to  
264  $\bar{z} = -\bar{z}'_0^+$  as

$$265 \quad \frac{\partial \tilde{h}_a}{\partial \bar{z}} - \frac{\partial \tilde{h}_b}{\partial \bar{z}} = \frac{\cos(\alpha_m \bar{x}'_0) K(\bar{y}'_0)}{p \kappa_z} \quad \text{at} \quad \bar{z} = -\bar{z}'_0 \quad (26)$$

266 Solving Eqs. (23) and (24) simultaneously with Eqs. (21), (22), (25), and (26) yields the  
267 Laplace-domain head solution as

$$268 \quad \tilde{h}_a(\alpha_m, \beta_n, \bar{z}, p) = \Omega(-\bar{z}'_0, \bar{z}, 1) \quad \text{for} \quad -\bar{z}'_0 \leq \bar{z} \leq 0 \quad (27a)$$

269 and

$$270 \quad \tilde{h}_b(\alpha_m, \beta_n, \bar{z}, p) = \Omega(\bar{z}, \bar{z}'_0, -1) \quad \text{for} \quad -1 \leq \bar{z} \leq -\bar{z}'_0 \quad (27b)$$

271 with

$$272 \quad \Omega(a, b, c) = \frac{\cosh[(1+a)\lambda] [-\kappa_z \lambda \cosh(b\lambda) + c p \gamma \sinh(b\lambda)] \cos(\alpha_m \bar{x}_0) K(\bar{y}_0)}{p \kappa_z \lambda (p \gamma \cosh \lambda + \kappa_z \lambda \sinh \lambda)} \quad (28)$$

$$273 \quad \lambda = \sqrt{(\kappa_x \alpha_m^2 + \beta_n^2 + p) / \kappa_z} \quad (29)$$

274 where  $a$ ,  $b$ , and  $c$  are arguments. Taking the inverse Laplace transform and finite integral  
275 transform to Eq. (28) results in Eq. (31). One is referred to Appendix B for the detailed  
276 derivation. A time-domain head solution for a point sink is therefore written as

$$277 \quad \bar{h}(\bar{x}, \bar{y}, \bar{z}, \bar{t}) = \begin{cases} \Phi(-\bar{z}'_0, \bar{z}, 1) & \text{for} \quad -\bar{z}'_0 \leq \bar{z} \leq 0 \\ \Phi(\bar{z}, \bar{z}'_0, -1) & \text{for} \quad -1 \leq \bar{z} \leq -\bar{z}'_0 \end{cases} \quad (30)$$



278 with

$$279 \quad \Phi(a, b, c) = \frac{2}{\bar{w}_x} \{ \sum_{n=1}^{\infty} [\phi_n X_n + 2 \sum_{m=1}^{\infty} \phi_{m,n} X_{m,n} \cos(\alpha_m \bar{x})] Y_n \} \quad (31)$$

$$280 \quad \phi_{m,n} = \psi_{m,n} + \psi_{m,n,0} + \sum_{i=1}^{\infty} \psi_{m,n,i} \quad (32)$$

$$281 \quad \psi_{m,n} = -\cosh[(1+a)\lambda_s] \cosh(b\lambda_s) / (\kappa_z \lambda_s \sinh \lambda_s) \quad (33)$$

$$282 \quad \psi_{m,n,0} = \mu_{m,n,0} \cosh[(1+a)\lambda_0] [-\kappa_z \lambda_0 \cosh(b\lambda_0) + c p_0 \gamma \sinh(b\lambda_0)] \quad (34)$$

$$283 \quad \psi_{m,n,i} = \nu_{m,n,i} \cos[(1+a)\lambda_i] [-\kappa_z \lambda_i \cos(b\lambda_i) + c p_i \gamma \sin(b\lambda_i)] \quad (35)$$

$$284 \quad \mu_{m,n,0} = 2 \exp(p_0 \bar{t}) / \{ p_0 [(1+2\gamma) \kappa_z \lambda_0 \cosh \lambda_0 + (p_0 \gamma + \kappa_z) \sinh \lambda_0] \} \quad (36)$$

$$285 \quad \nu_{m,n,i} = 2 \exp(p_i \bar{t}) / \{ p_i [(1+2\gamma) \kappa_z \lambda_i \cos \lambda_i + (p_i \gamma + \kappa_z) \sin \lambda_i] \} \quad (37)$$

$$286 \quad Y_n = \frac{\beta_n \cos(\beta_n \bar{y}) + \kappa_1 \sin(\beta_n \bar{y})}{(\beta_n^2 + \kappa_1^2) [\bar{w}_y + \kappa_2 / (\beta_n^2 + \kappa_2^2)] + \kappa_1} \quad (38)$$

287 and

$$288 \quad X_{m,n} = \cos(\alpha_m \bar{x}'_0) [\beta_n \cos(\beta_n \bar{y}'_0) + \kappa_1 \sin(\beta_n \bar{y}'_0)] \quad (39)$$

289 where  $\lambda_s = \sqrt{(\kappa_x \alpha_m^2 + \beta_n^2) / \kappa_z}$ ,  $p_0 = \kappa_z \lambda_0^2 - \kappa_x \alpha_m^2 - \beta_n^2$ ,  $p_i = -\kappa_z \lambda_i^2 - \kappa_x \alpha_m^2 - \beta_n^2$ ,  $\phi_n$

290 and  $X_n$  equal  $\phi_{m,n}$  and  $X_{m,n}$  with  $\alpha_m = 0$ , respectively, and the eigenvalues  $\lambda_0$  and  $\lambda_i$  are,

291 respectively, the roots of the following equations:

$$292 \quad e^{2\lambda_0} = \frac{-\gamma \kappa_z \lambda_0^2 + \kappa_z \lambda_0 + \gamma (\kappa_x \alpha_m^2 + \beta_n^2)}{\gamma \kappa_z \lambda_0^2 + \kappa_z \lambda_0 - \gamma (\kappa_x \alpha_m^2 + \beta_n^2)} \quad (40)$$

$$293 \quad \tan \lambda_i = \frac{-\gamma (\kappa_z \lambda_i^2 + \kappa_x \alpha_m^2 + \beta_n^2)}{\kappa_z \lambda_i} \quad (41)$$

294 The determination for those eigenvalues is introduced in the next section. Notice that the

295 solution consists of simple series expanded in  $\beta_n$ , double series expanded in  $\beta_n$  and  $\lambda_i$  (or

296  $\alpha_m$  and  $\beta_n$ ), and triple series expanded in  $\alpha_m$ ,  $\beta_n$  and  $\lambda_i$ .

### 297 2.3 Evaluations for $\beta_n$ , $\lambda_0$ and $\lambda_i$

298 Application of Newton's method with proper initial guesses to determine the eigenvalues

299  $\beta_n$ ,  $\lambda_0$  and  $\lambda_i$  has been proposed by Huang et al. (2014) and is briefly introduced herein. The

300 eigenvalues are situated at the intersection points of the left-hand side (LHS) and RHS  
 301 functions of Eq. (19) for  $\beta_n$ , Eq. (40) for  $\lambda_0$ , and Eq. (41) for  $\lambda_i$ . Hence, the initial guesses  
 302 for  $\beta_n$  are considered as  $\beta_v - \delta$  if  $\beta_v > (\kappa_1 \kappa_2)^{0.5}$  and as  $\beta_v + \delta$  if  $\beta_v < (\kappa_1 \kappa_2)^{0.5}$   
 303 where  $\beta_v = (2n - 1)\pi/(2 \bar{w}_y)$  and  $\delta$  is a chosen small value such as  $10^{-8}$  for avoiding being  
 304 right at the vertical asymptote. In addition, the guess for  $\lambda_0$  can be formulated as

$$305 \lambda_{0 \text{ initial}} = \delta + \{-\kappa_z - \sqrt{\kappa_z[\kappa_z + 4 \gamma^2(\kappa_x \alpha_m^2 + \beta_n^2)]}\}/(2\gamma\kappa_z) \quad (42)$$

306 where the RHS second term represents the location of the vertical asymptote derived by letting  
 307 the denominator of the RHS function in Eq. (40) to be zero and solving  $\lambda_0$  in the resultant  
 308 equation. Moreover, the guessed value for  $\lambda_i$  is  $(2i - 1)\pi/2 + \delta$ .

#### 309 **2.4 Head solution for radial collector well**

310 The lateral of RCW is approximately represented by a line sink composed of a series of  
 311 adjoining point sinks. The locations of these point sinks are expressed in terms of  $(\bar{x}_0 + \bar{l} \cos \theta,$   
 312  $\bar{y}_0 + \bar{l} \sin \theta, \bar{z}_0)$  where  $(\bar{x}_0, \bar{y}_0, \bar{z}_0) = (x_0/y_0, 1, z_0/H)$  is the central of the lateral, and  $\bar{l}$  is  
 313 a variable to define different locations of the point sink. The solution of head  $\bar{h}_w(\bar{x}, \bar{y}, \bar{z}, \bar{t})$  for  
 314 a lateral can therefore be derived by substituting  $\bar{x}'_0 = \bar{x}_0 + \bar{l} \cos \theta$ ,  $\bar{y}'_0 = 1 + \bar{l} \sin \theta$  and  
 315  $\bar{z}'_0 = \bar{z}_0$  into the point-sink solution, Eq. (30), then by integrating the resultant solution to  $\bar{l}$ ,  
 316 and finally by dividing the integration result into the sum of lateral lengths. The derivation can  
 317 be denoted as

$$318 \bar{h}_w(\bar{x}, \bar{y}, \bar{z}, \bar{t}) = (\sum_{k=1}^N \bar{L}_k)^{-1} \sum_{k=1}^N \int_0^{\bar{L}_k} \bar{h}(\bar{x}, \bar{y}, \bar{z}, \bar{t}) d\bar{l} \quad (43)$$

319 where  $\bar{L}_k = L_k/y_0$  is the  $k$ -th dimensionless lateral length. Note that the integration variable  
 320  $\bar{l}$  (i.e.,  $\bar{x}'_0$  and  $\bar{y}'_0$ ) appears only in  $X_n$  and  $X_{m,n}$  in Eq. (31). The integral in Eq. (43) can  
 321 thus be done analytically by integrating  $X_n$  and  $X_{m,n}$  with respect to  $\bar{l}$ . After the integration,  
 322 Eq. (43) can be expressed as

$$323 \bar{h}_w(\bar{x}, \bar{y}, \bar{z}, \bar{t}) = (\sum_{k=1}^N \bar{L}_k)^{-1} \sum_{k=1}^N \begin{cases} \Phi(-\bar{z}_0, \bar{z}, 1) & \text{for } -\bar{z}_0 \leq \bar{z} \leq 0 \\ \Phi(\bar{z}, \bar{z}_0, -1) & \text{for } -1 \leq \bar{z} \leq -\bar{z}_0 \end{cases} \quad (44)$$

324 where  $\Phi$  is defined by Eqs. (31) – (38), and  $X_n$  and  $X_{m,n}$  in Eq. (31) are replaced,

325 respectively, by

$$326 \quad X_{n,k} = -G_k / (\beta_n \sin \theta_k) \quad (45)$$

327 and

$$328 \quad X_{m,n,k} = \frac{\alpha_m F_k \cos \theta_k + \beta_n G_k \sin \theta_k}{\alpha_m^2 \cos^2 \theta_k - \beta_n^2 \sin^2 \theta_k} \quad (46)$$

329 with

$$330 \quad F_k = \sin(X\alpha_m)[\beta_n \cos(Y\beta_n) + \kappa_1 \sin(Y\beta_n)] - \sin(\bar{x}_0\alpha_m)(\beta_n \cos \beta_n + \kappa_1 \sin \beta_n) \quad (47)$$

$$331 \quad G_k = \cos(X\alpha_m)[\kappa_1 \cos(Y\beta_n) - \beta_n \sin(Y\beta_n)] - \cos(\bar{x}_0\alpha_m)(\kappa_1 \cos \beta_n - \beta_n \sin \beta_n) \quad (48)$$

332 where  $X = \bar{x}_0 + \bar{L}_k \cos \theta_k$  and  $Y = 1 + \bar{L}_k \sin \theta_k$ . Notice that Eq. (45) is obtained by

333 substituting  $\alpha_m = 0$  into Eq. (46). When  $\theta_k = 0$  or  $\pi$ , Eq. (45) reduces to Eq. (49) by

334 applying L'Hospital's rule.

$$335 \quad X_{n,k} = \bar{L}_k (\beta_n \cos \beta_n + \kappa_1 \sin \beta_n) \quad (49)$$

### 336 2.5 SDR solution for radial collector well

337 On the basis of Darcy's law and the head solution for a RCW, the SDR from streams 1

338 and 2 can be defined, respectively, as

$$339 \quad SDR_1(\bar{t}) = - \int_{\bar{x}=0}^{\bar{x}=\bar{w}_x} \left( \int_{\bar{z}=-\bar{z}_0}^{\bar{z}=0} \frac{\partial \bar{h}_w}{\partial \bar{y}} d\bar{z} + \int_{\bar{z}=-1}^{\bar{z}=-\bar{z}_0} \frac{\partial \bar{h}_w}{\partial \bar{y}} d\bar{z} \right) d\bar{x} \quad \text{at } \bar{y} = 0 \quad (50)$$

340 and

$$341 \quad SDR_2(\bar{t}) = \int_{\bar{x}=0}^{\bar{x}=\bar{w}_x} \left( \int_{\bar{z}=-\bar{z}_0}^{\bar{z}=0} \frac{\partial \bar{h}_w}{\partial \bar{y}} d\bar{z} + \int_{\bar{z}=-1}^{\bar{z}=-\bar{z}_0} \frac{\partial \bar{h}_w}{\partial \bar{y}} d\bar{z} \right) d\bar{x} \quad \text{at } \bar{y} = \bar{w}_y \quad (51)$$

342 Again, the double integrals in both equations can be done analytically. Notice that the series

343 term of  $2 \sum_{m=1}^{\infty} \phi_{m,n} X_{m,n} \cos(\alpha_m \bar{x})$  in Eq. (31) disappears due to the consideration of Eqs.

344 (3) and (4) and the integration with respect to  $\bar{x}$  in Eqs. (50) and (51) when deriving the SDR

345 solution. The  $SDR_1$  and  $SDR_2$  are therefore expressed in terms of double series and given below:

$$346 \quad SDR_1(\bar{t}) = - \frac{2}{\sum_{k=1}^N \bar{L}_k} \sum_{k=1}^N \sum_{n=1}^{\infty} (\psi'_n + \psi'_{n,0} + \sum_{i=1}^{\infty} \psi'_{n,i}) X_{n,k} Y'_n(0) \quad (52)$$

347 and

$$348 \quad SDR_2(\bar{t}) = \frac{2}{\sum_{k=1}^N L_k} \sum_{k=1}^N \sum_{n=1}^{\infty} (\psi'_n + \psi'_{n,0} + \sum_{i=1}^{\infty} \psi'_{n,i}) X_{n,k} Y'_n(\bar{w}_y) \quad (53)$$

349 with

$$350 \quad Y'_n(\bar{y}) = \frac{\kappa_1 \beta_n \cos(\beta_n \bar{y}) - \beta_n^2 \sin(\beta_n \bar{y})}{(\beta_n^2 + \kappa_1^2)[\bar{w}_y + \kappa_2 / (\beta_n^2 + \kappa_2^2)] + \kappa_1} \quad (54)$$

$$351 \quad \psi'_n = -\{\sinh(\bar{z}_0 \lambda'_s) \cosh[(1 - \bar{z}_0) \lambda'_s] + \sinh[(1 - \bar{z}_0) \lambda'_s] \cosh(\bar{z}_0 \lambda'_s)\} / (\kappa_z \lambda'^2_s \sinh \lambda'_s) \\ 352 \quad (55)$$

$$353 \quad \psi'_{n,0} = -\mu_{n,0}(\theta_{n,0} + \vartheta_{n,0}) / \lambda_0 \quad (56)$$

$$354 \quad \theta_{n,0} = \cosh[(1 - \bar{z}_0) \lambda_0] \{p'_0 \gamma [-1 + \cosh(\bar{z}_0 \lambda_0) + \kappa_z \lambda_0 \sinh(\bar{z}_0 \lambda_0)]\} \quad (57)$$

$$355 \quad \vartheta_{n,0} = \sinh[(1 - \bar{z}_0) \lambda_0] [\kappa_z \lambda_0 \cosh(\bar{z}_0 \lambda_0) + p'_0 \gamma \sinh(\bar{z}_0 \lambda_0)] \quad (58)$$

$$356 \quad \psi'_{n,i} = v_{n,i}(\sigma_{n,i} - \eta_{n,i}) / \lambda_i \quad (59)$$

$$357 \quad \sigma_{n,i} = \cos[(1 - \bar{z}_0) \lambda_i] \{p'_i \gamma [-1 + \cos(\bar{z}_0 \lambda_i)] - \kappa_z \lambda_i \sin(\bar{z}_0 \lambda_i)\} \quad (60)$$

$$358 \quad \eta_{n,i} = \sin[(1 - \bar{z}_0) \lambda_i] [\kappa_z \lambda_i \cos(\bar{z}_0 \lambda_i) + p'_i \gamma \sin(\bar{z}_0 \lambda_i)] \quad (61)$$

359 where  $\lambda'_s = \beta_n / \sqrt{\kappa_z}$ ;  $p'_0 = \kappa_z \lambda_0^2 - \beta_n^2$ ;  $p'_i = -\kappa_z \lambda_i^2 - \beta_n^2$ ;  $\mu_{n,0}$  equals  $\mu_{m,n,0}$  in Eq. (36)

360 with  $\alpha_m = 0$ ;  $v_{n,i}$  equals  $v_{m,n,i}$  in Eq. (37) with  $\alpha_m = 0$ ;  $X_{n,k}$  is defined in Eq. (45) for

361  $\theta_k \neq 0$  or  $\pi$  and Eq. (49) for  $\theta_k = 0$  or  $\pi$ ; and  $\lambda_0$  and  $\lambda_i$  are the roots of Eqs. (40) and

362 (41) with  $\alpha_m = 0$ , respectively.

363

## 364 2.6 Special cases of the present solution

### 365 2.6.1 Confined aquifer of finite extent

366 If  $\gamma = 0$  (i.e.,  $S_y = 0$  in Eq. (8)), the top boundary is regarded as an impermeable stratum.

367 The aquifer is then a confined system. Under this circumstance, Eq. (40) reduces to  $e^{2\lambda_0} = 1$

368 having the root of  $\lambda_0 = 0$ , and Eq. (41) yields  $\tan \lambda_i = 0$  having the roots of  $\lambda_i = i \pi$  where

369  $i \in 1, 2, 3, \dots, \infty$ . With  $\gamma = 0$ ,  $\lambda_0 = 0$  and  $\lambda_i = i \pi$ , the head solution for a confined aquifer

370 can be expressed as Eq. (44) with Eqs. (31) – (38) and (45) – (49) where  $\psi_{m,n,0}$  in Eq. (32)

371 is replaced by

$$372 \quad \psi_{m,n,0} = -\exp(p_0 \bar{t})/p_0 \quad (62)$$

373 Similarly, the SDR solution for a confined aquifer can be written as Eqs. (52) and (53) where  
374 the RHS function in Eq. (56) reduces to that in Eq. (62) by applying L'Hospital's rule with  $\gamma =$   
375  $0$  and  $\lambda_0 = 0$ .

### 376 **2.6.2 Confined aquifer of infinite extent**

377 The head solution introduced in section 2.6.1 is applicable to spatiotemporal head  
378 distributions in confined aquifers of infinite extent before the lateral boundary effect comes.  
379 Wang and Yeh (2008) indicated that the time can be quantified, in our notation, as  $t = R^2 S_y / (16 K_y)$   
380 (i.e.,  $\bar{t} = R^2 / (16 y_0^2)$  for dimensionless time) where  $R$  is the shortest distance between a RCW  
381 and aquifer lateral boundary. Prior to the time, the present head solution with  $N = 1$  for a  
382 horizontal well in a confined aquifer gives very close results given in Zhan et al. (2001).

### 383 **2.6.3 Unconfined aquifer of infinite extent**

384 Prior to the beginning time mentioned in section 2.6.2, the absolute value calculated by  
385 the present head solution, Eqs. (44) with  $N = 1$ , represents drawdown induced by a horizontal  
386 well in unconfined aquifers of infinite extent. The calculated drawdown should be close to that  
387 from Zhan and Zlotnik (2002) solution for the case of the instantaneous drainage from water  
388 table decline.

### 389 **2.6.4 Unconfined aquifer of semi-infinite extent**

390 When  $\kappa_1 \rightarrow \infty$  (i.e.,  $b_1 = 0$ ), Eq. (14) reduces to the Dirichlet condition of  $\bar{h} = 0$  for stream  
391 1 in the absence from a low-permeability streambed, and Eq. (19) becomes  $\tan(\beta_n \bar{w}_y) =$   
392  $-\beta_n / \kappa_2$ . In addition, the boundary effect occurring at the other three sides of the aquifer can  
393 be neglected prior to the beginning time. Moreover, when  $N = 1$  and  $\theta_1 = 0$ , a RCW can be  
394 regarded as a horizontal well parallel to stream 1. Under these three conditions, the present  
395 head and SDR predictions are close to those in Huang et al. (2011), the head solution of which

396 agrees well with measured data from a field experiment executed by Mohamed and Rushton  
 397 (2006). On the other hand, before the time when the boundary effect occurs at  $\bar{x} = 0$ ,  $\bar{x} = \bar{w}_x$   
 398 and  $\bar{y} = \bar{w}_y$ , the present head and SDR solutions for a RCW give close predictions to those in  
 399 Huang et al. (2012), the head and SDR solutions of which agree well with observation data  
 400 taken from two field experiments carried out by Schafer (2006) and Jasperse (2009),  
 401 respectively.

## 402 2.7 Sensitivity analysis

403 The hydraulic parameters determined from field observed data are inevitably subject to  
 404 measurement errors. Consequently, head predictions from the analytical model have  
 405 uncertainty due to the propagation of measurement errors. Sensitivity analysis can be  
 406 considered as a tool of exploring the response of the head to the change in a specific parameter  
 407 (Zheng and Bennett, 2002). One may define the normalized sensitivity coefficient as

$$408 S_{i,t} = \frac{P_i}{H} \frac{\partial h}{\partial P_i} \quad (63)$$

409 where  $S_{i,t}$  is the normalized sensitivity coefficient for the  $i$ th parameter at time  $t$ , and  $P_i$   
 410 represents the magnitude of the  $i$ th parameter. Eq. (63) can be approximated as

$$411 S_{i,t} = \frac{h(P_i + \Delta P_i) - h(P_i)}{\Delta P_i} \times \frac{P_i}{H} \quad (64)$$

412 where  $\Delta P_i$  is an increment chosen as  $10^{-3} P_i$  (Yeh et al., 2008).

## 413 3. Results and discussion

414 This section demonstrates head and SDR predictions and explores some physical insights  
 415 regarding flow behavior. In section 3.1, ~~groundwater flow and equipotential lines induced by~~  
 416 ~~pumping are drawn discussed to identify 3-D or 2-D flow without the vertical flow at a specific~~  
 417 ~~region~~. In section 3.2, the influence of anisotropy on spatial head and temporal SDR  
 418 distributions is studied. In section 3.3, the sensitivity analysis is performed to investigate the  
 419 response of the head to the change in each hydraulic parameter. In section 3.4, the effects of

420 the vertical flow and well depth on temporal SDR distributions for confined and unconfined  
 421 aquifers are investigated. For conciseness, we consider a RCW with two laterals with  $N = 2$ ,  
 422  $\bar{L}_1 = \bar{L}_2 = 0.5$ ,  $\theta_1 = 0$  and  $\theta_2 = \pi$ . The well can be viewed as a horizontal well parallel to  
 423 streams 1 and 2. The default values for the other dimensionless parameters are  $\bar{w}_x = \bar{w}_y = 2$ ,  
 424  $\gamma = 100$ ,  $\bar{x}_0 = 1$ ,  $\bar{y}_0 = 1$ ,  $\bar{z}_0 = 0.5$ ,  $\kappa_x = \kappa_z = 1$ , and  $\kappa_1 = \kappa_2 = 20$ .

425 **3.1 Identification of 3-D or 2-D flow at observation point**~~Groundwater flow and hydraulic~~  
 426 ~~head~~

427 Most existing models assume 2-D flow with neglecting the vertical flow for pumping at a  
 428 horizontal well (e.g., Mohamed and Rushton, 2006; Haitjema et al., 2010). The head  
 429 distributions predicted by those models are inaccurate if an observation ~~point~~well is close to  
 430 the region where the vertical flow prevails. Figure 2 demonstrates the ~~streamlines and~~  
 431 equipotential lines predicted by the present solution for a horizontal well in an unconfined  
 432 aquifer for  $\bar{x}_0 = 10$ ,  $\bar{w}_x = \bar{w}_y = 20$  and  $\kappa_z = 0.1, 1$ , and  $10$ . The well is located at  $9.5 \leq$   
 433  $\bar{x} \leq 10.5$ ,  $\bar{y} = 1$  and  $\bar{z} = 0.5$  as illustrated in the figure. The equipotential lines are based  
 434 on steady-state head distributions plotted by Eq. (44) with  $\bar{y} = 1$  and  $\bar{t} = 10^7$ . ~~The stream~~  
 435 ~~function  $\bar{\psi}$  can be derived via the Cauchy-Riemann equation, in our notation, as~~

$$\frac{\partial \bar{\psi}}{\partial \bar{x}} = -\sqrt{\kappa_z} \frac{\partial \bar{h}_w}{\partial \bar{z}} \quad (65)$$

437 where  ~~$\bar{\psi} = K_y H \psi / Q$  is the dimensionless stream function describing 2-D streamlines at~~  
 438 ~~the vertical plane of  $\bar{y} = 1$  based on  $\bar{h}_w$  in Eq. (44) with  $\bar{t} = 10^7$  for steady state. The~~  
 439 ~~function  $\bar{\psi}$  is obtained firstly by substituting Eq. (44) into Eq. (65), then by differentiating the~~  
 440 ~~result with respect to  $\bar{z}$ , and eventually by integrating the differentiation result to  $\bar{x}$ . The~~  
 441 ~~coefficient arising from the integration is determined by the condition of  $\bar{\psi} = 0$  at  $\bar{x} = \bar{x}_0$ .~~  
 442 ~~The detailed derivation of the stream function is shown in Appendix C.~~ When  $\kappa_z = 0.1$ , in the  
 443 range of  $10 \leq \bar{x} \leq 13.66$ , the contours of the hydraulic head are in a curved path, and the flow

格式化: 缩排: 第一行: 2 字元, 定位停駐點: 不在 36.5 字元

格式化: 缩排: 第一行: 2 字元

444 toward the well is thus slanted. Moreover, the range decreases to  $10 \leq \bar{x} \leq 11.5$  when  $\kappa_z = 1$   
445 and to  $10 \leq \bar{x} \leq 10.82$  when  $\kappa_z = 10$ . Beyond these ranges, the head contours are nearly vertical,  
446 and the flow is essentially horizontal. Define  $\bar{d} = d/y_0$  as a shortest dimensionless horizontal  
447 distance between the well and a nearest location of only horizontal flow. The  $\bar{d}$  is therefore  
448 chosen as 3.16, 1 and 0.32 for the cases of  $\kappa_z = 0.1, 1$  and  $10$ , respectively. Substituting  $(\kappa_z, \bar{d})$   
449  $= (0.1, 3.16), (1, 1)$  and  $(10, 0.32)$  into  $\kappa_z \bar{d}^2$  leads to about unity. We may therefore conclude  
450 that the vertical flow at an observation ~~location-point~~ is negligible if its location is beyond the  
451 range  
452 of  
453 a shortest dimensionless horizontal distance between the location and a RCW is less than  $\bar{d}$   
454  $\leq \sqrt{1/\kappa_z}$  (i.e.,  $d \leq H\sqrt{K_y/K_z}$ ) for thin aquifers, an observation ~~locations-point~~ far from  
455 the well, and/or a small ratio of  $K_y/K_z$ .

### 456 3.2 Anisotropy analysis of hydraulic head and stream depletion rate

457 Previous articles have seldom analyzed flow behavior for anisotropic aquifers, i.e.,  $\kappa_x$   
458  $(K_x/K_y) \neq 1$ . Head predictions based on the models, developed for isotropic aquifers, will be  
459 inaccurate if  $\kappa_x \neq 1$ . Consider  $\bar{w}_x = \bar{w}_y = 2$ ,  $\bar{t} = 10^7$  for steady-state head distributions, and  
460 a RCW with  $\bar{L}_1 = \bar{L}_2 = 0.25$ ,  $\theta_1 = 0$ ,  $\theta_2 = \pi$ , and  $(\bar{x}_0, \bar{y}_0, \bar{z}_0) = (1, 1, -0.5)$  for symmetry. The  
461 contours of the dimensionless head at  $\bar{z} = -0.5$  are shown in Figures 3(a) – 3(d) for  $\kappa_x = 1$ ,  
462  $10$  and  $50$ ,  $10^{-3}$ , and  $10^{-4}$ , respectively. The figure indicates that the anisotropy causes a  
463 significant effect on the head distributions in comparison with the case of  $\kappa_x = 1$ . In Figure 3(b),  
464 the contours exhibit smooth curves in the strip regions of  $1 \leq \bar{y} \leq 1.45$  for the case of  $\kappa_x = 10$   
465 and  $1 \leq \bar{y} \leq 1.2$  for the case of  $\kappa_x = 50$ . For the region of  $\bar{y} \geq 1.45$ , the predicted heads for  
466 both cases agree well, and all the contour lines are parallel, indicating that the flow is essentially  
467 unidirectional. Substituting  $(\kappa_x, \bar{y}) = (10, 1.45)$  and  $(50, 1.2)$  into  $\kappa_x (\bar{y} - 1)^2$  results in a value



468 about 2. Accordingly, we may draw the conclusion that plots from the inequality of  
 469  $\kappa_x (\bar{y} - 1)^2 \leq 2$  indicate the strip region for  $\kappa_x$  being greater than 10. Some existing models  
 470 assuming 2-D flow in a vertical plane with neglecting the flow component along a horizontal  
 471 well give accurate head predictions beyond the region (e.g., Anderson, 2000; Anderson, 2003;  
 472 Kompani-Zare et al., 2005).

473 Aquifers with  $K_y H \geq 10^3$  m<sup>2</sup>/day can efficiently produce plenty of water from a well.  
 474 RCWs usually operate with  $Q \leq 10^5$  m<sup>3</sup>/day for field experiments (e.g., Schafer, 2006; Jasperse,  
 475 2009). We therefore define significant dimensionless head drop as  $|\bar{h}| > 10^{-5}$  (i.e.,  $|h| > 1$   
 476 mm). The anisotropy of  $\kappa_x < 1$  produces the drop in the strip areas of  $1 \leq \bar{x} \leq 1.48$  for the case  
 477 of  $\kappa_x = 10^{-3}$  in Figure 3(c) and  $1 \leq \bar{x} \leq 1.32$  for the case of  $\kappa_x = 10^{-4}$  in Figure 3(d).  
 478 Substituting  $(\kappa_x, \bar{x}) = (10^{-3}, 1.48)$  and  $(10^{-4}, 1.32)$  into  $(\bar{x} - \bar{x}_0 - \bar{L}_1)^2 / \kappa_x$  approximates 52.9.  
 479 This result leads to the conclusion that the area can be determined by the inequalities of  
 480  $(\bar{x} - \bar{x}_0 - \bar{L}_1)^2 \leq 52.9\kappa_x$  and  $(\bar{x} - \bar{x}_0 + \bar{L}_2)^2 \leq 52.9\kappa_x$  for any value of  $\kappa_x$  in the range  $\kappa_x < 1$ .  
 481 For a RCW with irregular lateral configurations, the inequalities become  $(\bar{x} - \max \bar{x}_k)^2 \leq$   
 482  $52.9\kappa_x$  and  $(\bar{x} - \min \bar{x}_k)^2 \leq 52.9\kappa_x$  where  $\bar{x}_k$  is coordinate  $\bar{x}$  of the far end of the  $k$ -th  
 483 lateral. The conclusion applies in principle to reduction in grid points for numerical solutions  
 484 based on finite difference methods or finite element methods. On the other hand, we have found  
 485 that Eq. (52) or (53) with various  $\kappa_x$  predicts the same temporal SDR distribution (not shown),  
 486 indicating that the SDR is independent of  $\kappa_x$ .

### 487 3.3 Sensitivity analysis of hydraulic head

488 Consider an unconfined aquifer of  $H = 20$  m and  $w_x = w_y = 800$  m with a RCW having  
 489 two laterals of  $L_1 = L_2 = 50$  m,  $\theta_1 = 0$  and  $\theta_2 = \pi$  and two piezometers installed at point A of  
 490 (400 m, 340 m, -10 m) and point B of (400 m, 80 m, -10 m) illustrated in Figure 4. As  
 491 discussed in section 3.1, the temporal head distribution at point A exhibits the unconfined  
 492 behavior in Figure 4(a) because of  $\kappa_x \bar{d}^2 < 1$  while at point B displays the confined one in Figure

493 4(b) due to  $\kappa_z \bar{d}^2 > 1$ . The sensitivity analysis is conducted with the aid of equation (64) to  
 494 observe head responses at these two piezometers to the change in each of  $K_x$ ,  $K_y$ ,  $K_z$ ,  $S_s$ ,  $S_y$ ,  $K_1$ ,  
 495  $L_1$  and  $z_0$ . The temporal distribution curves of the normalized sensitivity coefficients for those  
 496 eight parameters are shown in Figures 4(a) for point A and 4(b) for point B when  $K_x = K_y = 1$   
 497 m/day,  $K_z = 0.1$  m/day,  $S_s = 10^{-5}$  m<sup>-1</sup>,  $S_y = 0.2$ ,  $K_1 = K_2 = 0.1$  m/day,  $b_1 = b_2 = 1$  m,  $Q = 100$   
 498 m<sup>3</sup>/day,  $x_0 = y_0 = 400$  m, and  $z_0 = 10$  m. The figure demonstrates that the hydraulic heads at  
 499 both piezometers are most sensitive to the change in  $K_y$ , second sensitive to the change in  $K_x$   
 500 and thirdly sensitive to the change in  $S_y$ , indicating that  $K_y$ ,  $K_x$  and  $S_y$  are the most crucial factors  
 501 in designing a pumping system. This figure also shows that the heads at point A is sensitive to  
 502 the change in  $S_s$  at the early period of  $4 \times 10^{-3}$  day  $< t < 10^{-1}$  day but at point B is insensitive to  
 503 the change over the entire period. In addition, the head at point A is sensitive to the changes in  
 504  $K_z$  and  $z_0$  due to 3-D flow (i.e.,  $\kappa_z \bar{d}^2 < 1$ ) as discussed in section 3.1. In contrast, the head at  
 505 point B is insensitive to the changes in  $K_z$  and  $z_0$  because the vertical flow diminishes (i.e.,  
 506  $\kappa_z \bar{d}^2 > 1$ ). Moreover, the head at point A is sensitive to the change in  $L_1$  but the head at point  
 507 B is not because its location is far away from the well. Furthermore, the normalized sensitivity  
 508 coefficient of  $K_1$  for point A away from stream 1 approaches zero but for point B in the vicinity  
 509 of stream 1 increases with time and finally maintains a certain value at the steady state.  
 510 Regarding the sensitivity analysis of SDR, Huang et al. (2014) has performed the sensitivity  
 511 analysis of normalized coefficients of  $SDR_1$  to the changes in  $K_y$ ,  $K_1$  and  $S_s$  for a confined  
 512 aquifer and in  $K_y$ ,  $K_z$ ,  $K_1$ ,  $S_s$  and  $S_y$  for an unconfined aquifer.

### 513 3.4 Effects of vertical flow and well depth on stream depletion rate

514 Huang et al. (2014) reveals that the effect of the vertical flow on SDR induced by a vertical  
 515 well is dominated by the magnitude of the key factor  $\kappa_z$  (i.e.,  $K_z \gamma_0^2 / (K_y H^2)$ ) where  $\gamma_0$  herein  
 516 is a distance between stream 1 and the vertical well. They concluded that the effect is negligible  
 517 when  $\kappa_z \geq 10$  for a leaky aquifer. The factor should be replaced by  $\kappa_z \bar{a}^2$  (i.e.,  $K_z \bar{a}^2 / (K_y H^2)$ )

518 where  $a$  is a shortest distance measured from stream 1 to the end of a lateral of a RCW, and  
 519  $\bar{a} = a/y_0 = 1$  in this study due to  $N = 2$ ,  $\theta_1 = 0$  and  $\theta_2 = \pi$ . We investigate SDR in response to  
 520 various  $\bar{z}_0$  and  $\kappa_z \bar{a}$  for unconfined and confined aquifers. The temporal SDR<sub>1</sub> distributions  
 521 predicted by Eq. (52) for stream 1 adjacent to an unconfined aquifer are shown in Fig. 5(a) for  
 522  $\bar{z}_0 = 0.5$  and  $\kappa_z \bar{a}^2 = 0.01, 0.1, 1, 10, 20$  and Fig. 5(b) for  $\kappa_z \bar{a}^2 = 1$  and 30 when  $\bar{z}_0 =$   
 523  $0.1, 0.3, 0.5, 0.7$  and  $0.9$ . The curves of SDR<sub>1</sub> versus  $\bar{t}$  is plotted in both panels by the present  
 524 SDR solution for a confined aquifer. In Fig. 5(a), the present solution for an unconfined aquifer  
 525 predicts a close SDR<sub>1</sub> to that for the confined aquifer when  $\kappa_z \bar{a}^2 = 0.01$ , indicating that the  
 526 vertical flow in the unconfined aquifer is ignorable. The SDR<sub>1</sub> for the unconfined aquifer with  
 527  $\kappa_z \bar{a}^2 = 30$  behaves like that for a confined one, indicating the vertical flow is also ignorable.  
 528 The SDR<sub>1</sub> is therefore independent of well depths  $\bar{z}_0$  when  $\kappa_z \bar{a}^2 = 30$  as shown in Fig. 5(b).  
 529 We may therefore conclude that, under the condition of  $\kappa_z \bar{a}^2 \leq 0.01$  or  $\kappa_z \bar{a}^2 \geq 30$ , a 2-D  
 530 horizontal flow model can give good predictions in SDR<sub>1</sub> for unconfined aquifers. In contrast,  
 531 SDR<sub>1</sub> increases with decreasing  $\kappa_z \bar{a}^2$  when  $0.01 < \kappa_z \bar{a}^2 < 30$  in Fig. 5(a), indicating that the  
 532 vertical flow component induced by pumping in unconfined aquifers significantly affects SDR<sub>1</sub>.  
 533 The effect of well depth  $\bar{z}_0$  on SDR<sub>1</sub> is also significant as shown in Fig. 5(b) when  $\kappa_z \bar{a}^2 = 1$ .  
 534 Obviously, the vertical flow effect should be considered in a model when  $0.01 < \kappa_z \bar{a}^2 < 30$   
 535 for unconfined aquifers.

536 It is interesting to note that the SDR<sub>1</sub> or SDR<sub>2</sub> induced by two laterals (i.e.,  $\theta_1 = 0$  and  $\theta_2$   
 537  $= \pi$ ) parallel to the streams adjacent to a confined aquifer is independent of  $\kappa_z \bar{a}^2$  and  $\bar{z}_0$  but  
 538 depends on aquifer width of  $\bar{w}_y$ . The temporal SDR distribution curves based on Eqs. (52) and  
 539 (53) with  $\gamma = 0$  for a confined aquifer with  $\bar{w}_y = 2, 4, 6, 10$  and  $20$  are plotted in Fig. 6. The  
 540 dimensionless distance between the well and stream 1 is set to unity (i.e.,  $\bar{y}_0 = 1$ ) for each  
 541 case. The SDR<sub>1</sub> predicted by Hunt (1999) solution based on a vertical well in a confined aquifer

542 extending infinitely is considered. The present solution for each  $\bar{w}_y$  gives the same  $SDR_1$  as  
543 the Hunt solution before the time when stream 2 contributes filtration water to the aquifer and  
544 influences the supply of  $SDR_1$ . It is interesting to note that the sum of steady-state  $SDR_1$  and  
545  $SDR_2$  is always unity for a fixed  $\bar{w}_y$ . The former and latter can be estimated by  $(\bar{w}_y - 1)/\bar{w}_y$   
546 and  $1/\bar{w}_y$ , respectively. Such a result corresponds with that in Sun and Zhan (2007) which  
547 investigates the distribution of steady-state  $SDR_1$  and  $SDR_2$  induced by a vertical well.

#### 548 **4. Concluding remarks**

549 This study develops a new analytical model describing 3-D flow induced by a RCW in a  
550 rectangular confined or unconfined aquifer bounded by two parallel streams and no-flow  
551 stratum in the other two sides. The flow equation in terms of the hydraulic head with a point  
552 sink term is employed. Both streams fully penetrate the aquifer and are under the Robin  
553 condition in the presence of low-permeability streambeds. A first-order free surface equation  
554 (8) describing the water table decline gives good predictions when the conditions  $|h|/H \leq 0.1$   
555 and  $|\partial h/\partial x| + |\partial h/\partial y| \leq 0.01$  are satisfied. The flux across the well screen might be  
556 uniform on a lateral within 150 m. The head solution for the point sink is expressed in terms of  
557 a triple series derived by the methods of Laplace transform and finite integral transform. The  
558 head solution for a RCW is then obtained by integrating the point-sink solution along the  
559 laterals and dividing the integration result by the sum of lateral lengths. The integration can be  
560 done analytically due to the aquifer of finite extent with Eqs. (3) – (6). On the basis of Darcy's  
561 law and the head solution, the  $SDR$  solution for two streams can also be acquired. The double  
562 integrals of defining the  $SDR$  in Eqs. (50) and (51) can also be done analytically due to  
563 considerations of Eqs. (3) – (6). The sensitivity analysis is performed to explore the response  
564 of the head to the change in each of the hydraulic parameters and variables. New findings  
565 regarding the responses of flow and  $SDR$  to pumping at a RCW are summarized below:

- 566 1. Groundwater flow in a region based on  $\bar{d} \leq \sqrt{1/\kappa_z}$  is 3-D, and temporal head  
567 distributions exhibit the unconfined behavior. A mathematical model should consider 3-D  
568 flow when predicting the hydraulic head in the region. Beyond this region, groundwater  
569 flow is horizontal, and temporal head distributions display the confined behavior. A 2-D  
570 flow model can predict accurate hydraulic head.
- 571 2. The aquifer anisotropy of  $\kappa_x > 10$  causes unidirectional flow in the strip region determined  
572 based on  $\kappa_x (\bar{y} - 1)^2 > 2$  for a horizontal well. Existing models assuming 2-D flow in a  
573 vertical plane with neglecting the flow component along the well give accurate head  
574 predictions in the region.
- 575 3. The aquifer anisotropy of  $\kappa_x < 1$  produces significant change in the head (i.e.,  $|\bar{h}| > 10^{-5}$   
576 or  $|h| > 1$  mm) in the strip area determined by  $(\bar{x} - \max \bar{x}_k)^2 \leq 52.9 \kappa_x$  and  $(\bar{x} -$   
577  $\min \bar{x}_k)^2 \leq 52.9 \kappa_x$  for a RCW with irregular lateral configurations.
- 578 4. The hydraulic head in the whole domain is most sensitive to the change in  $K_y$ , second  
579 sensitive to the change in  $K_x$ , and thirdly sensitive to the change in  $S_y$ . They are thus the  
580 most crucial factors in designing a pumping system.
- 581 5. The hydraulic head is sensitive to changes in  $K_z$ ,  $S_s$ ,  $z_0$  and  $L_k$  in the region of  $\bar{d} <$   
582  $\sqrt{1/\kappa_z}$  and is insensitive to the changes of them beyond the region.
- 583 6. The hydraulic head at observation ~~locations~~ points near stream 1 is sensitive to the change  
584 in  $K_1$  but away from the stream isn't.
- 585 7. The effect of the vertical flow on SDR is ignorable when  $\kappa_z \bar{a}^2 \leq 0.01$  or  $\kappa_z \bar{a}^2 \geq 30$  for  
586 unconfined aquifers. In contrast, neglecting the effect will underestimate SDR when  $0.01$   
587  $< \kappa_z \bar{a}^2 < 30$ .
- 588 8. For unconfined aquifers, SDR increases with dimensionless well depth  $\bar{z}_0$  when  $0.01 < \kappa_z$   
589  $< 30$  and is independent of  $\bar{z}_0$  when  $\kappa_z \leq 0.01$  or  $\kappa_z \geq 30$ . For confined aquifers, SDR is

590 independent of  $\bar{z}_0$  and  $\kappa_z$ . For both kinds of aquifers, the distribution curve of SDR versus  
 591  $\bar{t}$  is independent of aquifer anisotropy  $\kappa_x$ .

592

593 **Acknowledgements.**

594 Research leading to this paper has been partially supported by the grants from the Taiwan  
 595 Ministry of Science and Technology under the contract NSC 102 – 2221 – E – 009 – 072 –  
 596 MY2, MOST 103 – 2221 – E – 009 – 156, and MOST 104 – 2221 – E – 009 – 148 – MY2.

597

598 **Appendix A: Finite integral transform**

599 Latinopoulos (1985) provided the finite integral transform for a rectangular aquifer  
 600 domain where each side can be under either the Dirichlet, no-flow, or Robin condition. The  
 601 transform associated with the boundary conditions, Eqs. (12) – (15), is defined as

$$602 \quad \tilde{h}(\alpha_m, \beta_n) = \mathfrak{S}\{\bar{h}(\bar{x}, \bar{y})\} = \int_0^{\bar{w}_x} \int_0^{\bar{w}_y} \bar{h}(\bar{x}, \bar{y}) \cos(\alpha_m \bar{x}) K(\bar{y}) d\bar{y} d\bar{x} \quad (\text{A1})$$

603 with

$$604 \quad K(\bar{y}) = \sqrt{2} \frac{\beta_n \cos(\beta_n \bar{y}) + \kappa_1 \sin(\beta_n \bar{y})}{\sqrt{(\beta_n^2 + \kappa_1^2)[\bar{w}_y + \kappa_2 / (\beta_n^2 + \kappa_2^2)] + \kappa_1}} \quad (\text{A2})$$

605 where  $\cos(\alpha_m \bar{x}) K(\bar{y})$  is the kernel function. According to Latinopoulos (1985, Eq. (9)), the  
 606 transform has the property of

$$607 \quad \mathfrak{S}\left\{\kappa_x \frac{\partial^2 \bar{h}}{\partial \bar{x}^2} + \frac{\partial^2 \bar{h}}{\partial \bar{y}^2}\right\} = -(\kappa_x \alpha_m^2 + \beta_n^2) \tilde{h}(\alpha_m, \beta_n) \quad (\text{A3})$$

608 The formula for the inverse finite integral transform can be written as (Latinopoulos, 1985, Eq.  
 609 (14))

$$610 \quad \bar{h}(\bar{x}, \bar{y}) = \mathfrak{S}^{-1}\{\tilde{h}(\alpha_m, \beta_n)\} = \frac{1}{\bar{w}_x} \left[ \sum_{n=1}^{\infty} \tilde{h}(0, \beta_n) K(\bar{y}) + 2 \sum_{m=1}^{\infty} \sum_{n=1}^{\infty} \tilde{h}(\alpha_m, \beta_n) \cos(\alpha_m \bar{x}) K(\bar{y}) \right] \quad (\text{A4})$$

611

612 **Appendix B: Derivation of equation (31)**

613 The function of  $p$  in Eq. (28) is defined as

$$614 \quad F(p) = \frac{\cosh[(1+a)\lambda] [-\kappa_z \lambda \cosh(b\lambda) + c p \gamma \sinh(b\lambda)]}{p \kappa_z \lambda (p \gamma \cosh \lambda + \kappa_z \lambda \sinh \lambda)} \quad (\text{B1})$$

615 Notice that the term  $\cos(\alpha_m \bar{x}_0) K(\bar{y}_0)$  in Eq. (28) is excluded because it is independent of  $p$ .

616  $F(p)$  is a single-value function with respect to  $p$ . On the basis of the residue theorem, the

617 inverse Laplace transform for  $F(p)$  equals the summation of residues of poles in the complex

618 plane. The residue of a simple pole can be derived according to the formula below:

$$619 \quad \text{Res}|_{p=p_i} = \lim_{p \rightarrow p_i} F(p) \exp(p\bar{t}) (p - p_i) \quad (\text{B2})$$

620 where  $p_i$  is the location of the pole in the complex plane.

621 The locations of poles are the roots of the equation obtained by letting the denominator in

622 Eq. (B1) to be zero, denoted as

$$623 \quad p \kappa_z \lambda (p \gamma \cosh \lambda + \kappa_z \lambda \sinh \lambda) = 0 \quad (\text{B3})$$

624 where  $\lambda$  is defined in Eq. (29). Notice that  $p = -\kappa_x \alpha_m^2 - \beta_n^2$  obtained by  $\lambda = 0$  is not a

625 pole in spite of being a root. Apparently, one pole is at  $p = 0$ , and the residue based on Eq. (B2)

626 with  $p_i = 0$  is expressed as

$$627 \quad \text{Res}|_{p=0} = \lim_{p \rightarrow 0} \frac{\cosh[(1+a)\lambda] [-\kappa_z \lambda \cosh(b\lambda) + c p \gamma \sinh(b\lambda)]}{\kappa_z \lambda (p \gamma \cosh \lambda + \kappa_z \lambda \sinh \lambda)} \exp(p\bar{t}) \quad (\text{B4})$$

628 Eq. (B4) with  $p = 0$  and  $\lambda = \lambda_s$  reduces to  $\psi_{m,n}$  in Eq. (33).

629 Other poles are determined by the equation of

$$630 \quad p \gamma \cosh \lambda + \kappa_z \lambda \sinh \lambda = 0 \quad (\text{B5})$$

631 which comes from Eq. (B3). One pole is at  $p = p_0$  between  $p = 0$  and  $p = -\kappa_x \alpha_m^2 - \beta_n^2$  in

632 the negative part of the real axis. Newton's method can be used to obtain the value of  $p_0$ . In

633 order to have proper initial guess for Newton's method, we let  $\lambda = \lambda_0$  and then have  $p =$

634  $\kappa_z \lambda_0^2 - \kappa_x \alpha_m^2 - \beta_n^2$  based on Eq. (29). Substituting  $\lambda = \lambda_0$ ,  $p = \kappa_z \lambda_0^2 - \kappa_x \alpha_m^2 - \beta_n^2$ ,

635  $\cosh \lambda_0 = (e^{\lambda_0} + e^{-\lambda_0})/2$  and  $\sinh \lambda_0 = (e^{\lambda_0} - e^{-\lambda_0})/2$  into Eq. (B5) and rearranging the

636 result leads to Eq. (40). Initial guess for finding root  $\lambda_0$  of Eq. (40) is discussed in section 2.3.

637 With known value of  $\lambda_0$ , one can obtain  $p_0 = \kappa_z \lambda_0^2 - \kappa_x \alpha_m^2 - \beta_n^2$ . According to Eq. (B2),

638 the residue of the simple pole at  $p = p_0$  is written as

$$639 \text{Res}|_{p=p_0} = \lim_{p \rightarrow p_0} \frac{\cosh[(1+a)\lambda][-\kappa_z \lambda \cosh(b\lambda) + c\gamma \sinh(b\lambda)]}{p\kappa_z \lambda (\gamma \cosh \lambda + \kappa_z \lambda \sinh \lambda)} \exp(p\bar{t}) (p - p_0) \quad (\text{B6})$$

640 where both the denominator and nominator equal zero when  $p = p_0$ . Applying L'Hospital's

641 Rule to Eq. (B6) results in

$$642 \text{Res}|_{p=p_0} = \lim_{p \rightarrow p_0} \frac{2\cosh[(1+a)\lambda][-\kappa_z \lambda \cosh(b\lambda) + c\gamma \sinh(b\lambda)]}{p[(1+2\gamma)\kappa_z \lambda \cosh \lambda + (\gamma p + \kappa_z) \sinh \lambda]} \exp(p\bar{t}) \quad (\text{B7})$$

643 Eq. (B7) with  $p = p_0$  and  $\lambda = \lambda_0$  reduces to  $\psi_{m,n,0}$  in Eq. (34).

644 On the other hand, infinite poles are at  $p = p_i$  behind  $p = -\kappa_x \alpha_m^2 - \beta_n^2$ . Similar to the

645 derivation of Eq. (40), we let  $\lambda = \sqrt{-1}\lambda_i$  and then have  $p = -\kappa_z \lambda_i^2 - \kappa_x \alpha_m^2 - \beta_n^2$  based

646 on Eq. (29). Substituting  $\lambda = \sqrt{-1}\lambda_i$ ,  $p = -\kappa_z \lambda_i^2 - \kappa_x \alpha_m^2 - \beta_n^2$ ,  $\cosh \lambda = \cos \lambda_i$  and

647  $\sinh \lambda = \sqrt{-1} \sin \lambda_i$  into Eq. (B3) and rearranging the result yields Eq. (41). The

648 determination of  $\lambda_i$  is discussed in section 2.3. With known value  $\lambda_i$ , one can have  $p_i =$

649  $-\kappa_z \lambda_i^2 - \kappa_x \alpha_m^2 - \beta_n^2$ . The residues of those simple poles at  $p=p_i$  can be expressed as  $\psi_{m,n,i}$

650 in Eq. (35) by substituting  $p_0 = p_i$ ,  $p = p_i$ ,  $\lambda = \sqrt{-1}\lambda_i$ ,  $\cosh \lambda = \cos \lambda_i$  and  $\sinh \lambda =$

651  $\sqrt{-1} \sin \lambda_i$  into Eq. (B7). Eventually, the inverse Laplace transform for  $F(p)$  equals the sum

652 of those residues (i.e.,  $\phi_{m,n} = \psi_{m,n} + \psi_{m,n,0} + \sum_{i=1}^{\infty} \psi_{m,n,i}$ ). The time-domain result of

653  $\Omega(a, b, c)$  in Eq. (28) is then obtained as  $\phi_{m,n} \cos(\alpha_m \bar{x}_0) K(\bar{y}_0)$ . By substituting

654  $\tilde{h}(\alpha_m, \beta_n) = \phi_{m,n} \cos(\alpha_m \bar{x}_0) K(\bar{y}_0)$  and  $\tilde{h}(0, \beta_n) = \phi_n K(\bar{y}_0)$  into Eq. (A4) and letting

655  $\bar{h}(\bar{x}, \bar{y})$  to be  $\Phi(a, b, c)$ , the inverse finite integral transform for the result can be derived as

$$656 \Phi(a, b, c) = \frac{1}{w_x} \left[ \sum_{n=1}^{\infty} (\phi_n K(\bar{y}_0) K(\bar{y}) + \right. \\ 657 \left. 2 \sum_{m=1}^{\infty} \phi_{m,n} \cos(\alpha_m \bar{x}_0) K(\bar{y}_0) \cos(\alpha_m \bar{x}) K(\bar{y}) \right] \quad (\text{B8})$$

658 Moreover, Eq. (B8) reduces to Eq. (31) when letting the terms of  $K(\bar{y}_0) K(\bar{y})$  and



659  $\cos(\alpha_m \bar{x}_0)K(\bar{y}_0)K(\bar{y})$  to be  $2X_n Y_n$  and  $2X_{m,n} Y_n$ , respectively.

660 **Appendix C: Derivation of  $\bar{\psi}$  in Eq. (65)**

661 The dimensionless stream function  $\bar{\psi}$  in Eq. (65) can be expressed as

662 
$$\bar{\psi} = C - \sqrt{\kappa_z} \int \partial \bar{h}_w / \partial \bar{z} d\bar{x} \text{ at } \bar{y} = 1 \text{ and } \bar{t} = 10^7 \quad (C1)$$

663 where  $C$  is a coefficient resulting from the integration, and  $\bar{h}_w$  is defined in Eq. (44).

664 Substituting Eq. (44) into Eq. (C1) leads to

665 
$$\bar{\psi}(\bar{x}, \bar{z}) = C - \frac{\sqrt{\kappa_z}}{\sum_{k=1}^N I_k} \sum_{k=1}^N \left\{ \int \frac{\partial \Phi(-\bar{z}_0, \bar{z}, 1) / \partial \bar{z} d\bar{x}}{\int \frac{\partial \Phi(\bar{z}, \bar{z}_0, -1) / \partial \bar{z} d\bar{x}}{\text{for } -1 \leq \bar{z} \leq -\bar{z}_0}} \text{ for } -\bar{z}_0 \leq \bar{z} \leq 0 \right. \\ \left. \int \frac{\partial \Phi(\bar{z}, \bar{z}_0, -1) / \partial \bar{z} d\bar{x}}{\text{for } -1 \leq \bar{z} \leq -\bar{z}_0}} \text{ for } -1 \leq \bar{z} \leq -\bar{z}_0 \right\} \text{ at } \bar{y} = 1 \text{ and } \bar{t} = 10^7 \quad (C2)$$

666 
$$\Phi(a, b, c) = \frac{2}{\bar{w}_x} \left\{ \sum_{n=1}^{\infty} [\phi_n X_{n,k} + 2 \sum_{m=1}^{\infty} \phi_{m,n} X_{m,n,k} \cos(\alpha_m \bar{x})] Y_n \right\} \quad (C3)$$

667 where  $\phi_{m,n}$ ,  $Y_n$ ,  $X_{n,k}$  and  $X_{m,n,k}$  are defined in Eqs. (32), (38), (45) and (46), respectively,

668 and  $\phi_n$  equals  $\phi_{m,n}$  with  $\alpha_m = 0$ . In Eq. (C3), variable  $\bar{x}$  appears only in  $\cos(\alpha_m \bar{x})$ , and

669 variable  $\bar{z}$  appears only in  $\phi_n$  and  $\phi_{m,n}$  in Eq. (32). Eq. (C2) therefore becomes

670 
$$\bar{\psi}(\bar{x}, \bar{z}) = C - \frac{\sqrt{\kappa_z}}{\sum_{k=1}^N I_k} \sum_{k=1}^N \left\{ \frac{\Phi^t(-\bar{z}_0, \bar{z}, 1)}{\Phi^t(-\bar{z}_0, \bar{z}, 1)} \text{ for } -\bar{z}_0 \leq \bar{z} \leq 0 \right. \\ \left. \frac{\Phi^t(-\bar{z}_0, \bar{z}, 1)}{\Phi^t(-\bar{z}_0, \bar{z}, 1)} \text{ for } -1 \leq \bar{z} \leq -\bar{z}_0} \right\} \text{ at } \bar{y} = 1 \text{ and } \bar{t} = 10^7 \quad (C4)$$

671 
$$\Phi^t(a, b, c) = \frac{2}{\bar{w}_x} \left\{ \sum_{n=1}^{\infty} \left[ \frac{\partial \phi_n}{\partial \bar{z}} X_{n,k} \int d\bar{x} + 2 \sum_{m=1}^{\infty} \frac{\partial \phi_{m,n}}{\partial \bar{z}} X_{m,n,k} \int \cos(\alpha_m \bar{x}) d\bar{x} \right] Y_n \right\} \quad (C5)$$

672 Consider  $\bar{t} = 10^7$  for steady state flow that the exponential terms of  $\exp(p_u \bar{t})$  and

673  $\exp(p_t \bar{t})$  approach zero (i.e.,  $p_u > 0$  and  $p_t > 0$ ) for the default values of the parameters

674 used to plot Figure 2. Then, we have  $\phi_{m,n} = \psi_{m,n}$  defined in Eq. (33) because of  $\psi_{m,n,0} \cong 0$ ,

675  $\psi_{m,n,t} \cong 0$ ,  $\mu_{m,n,u} \cong 0$  and  $\nu_{m,n,t} \cong 0$ . On the basis of  $\phi_{m,n} = \psi_{m,n}$  and Eq. (33) with  $a =$

676  $-\bar{z}_0$  and  $b = \bar{z}$  for  $-\bar{z}_0 \leq \bar{z} \leq 0$  and  $a = \bar{z}$  and  $b = \bar{z}_0$  for  $-1 \leq \bar{z} \leq -\bar{z}_0$ , the result of

677 differentiation, i.e.,  $\partial \phi_{m,n} / \partial \bar{z}$ , in Eq. (C5) equals

678 
$$\frac{\partial \phi_{m,n}}{\partial \bar{z}} = \begin{cases} -\lambda_s \cosh[(1 - \bar{z}_0)\lambda_s] \sinh(\bar{z} \lambda_s) / (\kappa_z \lambda_s \sinh \lambda_s) & \text{for } -\bar{z}_0 \leq \bar{z} \leq 0 \\ (-\lambda_s \sinh[(1 + \bar{z})\lambda_s] \cosh(\bar{z}_0 \lambda_s) / (\kappa_z \lambda_s \sinh \lambda_s) & \text{for } -1 \leq \bar{z} \leq -\bar{z}_0 \end{cases} \quad (C6)$$

679 Notice that  $\partial \phi_n / \partial \bar{z}$  in Eq. (C5) equals Eq. (C6) with  $\alpha_m = 0$ . In addition, both integrations

680 in Eq. (C5) can be done analytically as

681 
$$f \cos(\alpha_m \bar{x}) d\bar{x} = \begin{cases} \frac{\sin(\alpha_m \bar{x}) / \alpha_m}{\bar{x}} \text{ for } \alpha_m \neq 0 \\ \bar{x} \text{ for } \alpha_m = 0 \end{cases} \quad (C7)$$

682 On the other hand, coefficient  $C$  in Eq. (C4) is determined by the condition of  $\bar{\psi} = 0$  at  $\bar{x} =$   
 683  $\bar{x}_0$  and results in

684 
$$C = \frac{\sqrt{k_z}}{\sum_{k=1}^N \bar{r}_k} \sum_{k=1}^N \begin{cases} \Phi^L(-\bar{z}_0, \bar{z}_k, 1) \text{ for } -\bar{z}_0 \leq \bar{z}_k \leq 0 \\ \Phi^L(-\bar{z}_0, \bar{z}_k, 1) \text{ for } -1 \leq \bar{z}_k \leq -\bar{z}_0 \end{cases} \quad (C8)$$

685 where  $\Phi^L$  is defined in Eq. (C5) with Eqs. (C6) and (C7),  $\bar{x} = \bar{x}_0$  and  $\bar{y} = 1$ .

686

687 **References**

688 Anderson, E. I.: The method of images for leaky boundaries, *Adv. Water Resour.*, 23, 461–474,  
 689 doi:10.1016/S0309-1708(99)00044-5, 2000.

690 Anderson, E. I.: An analytical solution representing groundwater-surface water interaction,  
 691 *Water Resour. Res.*, 39(3), 1071, doi:10.1029/2002WR001536, 2003.

692 Anderson, E. I.: Stable pumping rates for horizontal wells in bank filtration systems, *Adv.*  
 693 *Water Resour.*, 54, 57–66, doi:10.1016/j.advwatres.2012.12.012, 2013.

694 Bear, J.: *Hydraulics of Groundwater*, McGraw-Hill, New York, 84, 1979.

695 Charbeneau, R. J.: *Groundwater Hydraulics and Pollutant Transport*, Prentice-Hall, NJ, 57,  
 696 2000.

697 Chen, C. X., Wan, J. W., and Zhan, H. B.: Theoretical and experimental studies of coupled  
 698 seepage-pipe flow to a horizontal well, *J. Hydrol.*, 281(1–2), 159–171,  
 699 doi:10.1016/S0022-1694(03)00207-5, 2003.

700 Chen, X., Dong, W., Ou, G., Wang, Z., and Liu, C.: Gaining and losing stream reaches have  
 701 opposite hydraulic conductivity distribution patterns, *Hydrol. Earth Syst. Sci.*, 17, 2569–  
 702 2579, doi:10.5194/hess-17-2569-2013, 2013.

703 Exner-Kittridge, M., Salinas, J. L., and Zessner, M.: An evaluation of analytical stream to  
 704 groundwater exchange models: a comparison of gross exchanges based on different spatial

705 flow distribution assumptions, *Hydrol. Earth Syst. Sci.*, 18, 2715–2734, doi:10.5194/hess-  
706 18-2715-2014, 2014.

707 Flipo, N., Mouhri, A., Labarthe, B., Biancamaria, S., Rivière, A., and Weill, P.: Continental  
708 hydrosystem modelling: the concept of nested stream–aquifer interfaces, *Hydrol. Earth*  
709 *Syst. Sci.*, 18, 3121–3149, doi:10.5194/hess-18-3121-2014, 2014.

710 Goldscheider, N., and Drew, D.: *Methods in karst hydrology*, Taylor & Francis Group, London,  
711 UK, 88, 2007.

712 Haitjema, H., Kuzin, S., Kelson, V., and Abrams, D.: Modeling flow into horizontal wells in a  
713 Dupuit-Forchheimer model, *Ground Water*, 48(6), 878–883, doi:10.1111/j.1745-  
714 6584.2010.00694.x, 2010.

715 Hantush, M. S. and Papadopoulos, I. S.: Flow of groundwater to collector wells, *J. Hydr. Eng.*  
716 *Div.*, 88(5), 221–244, 1962.

717 Huang, C. S., Chen, Y. L., and Yeh, H. D.: A general analytical solution for flow to a single  
718 horizontal well by Fourier and Laplace transforms, *Adv. Water Resour.*, 34(5), 640–648,  
719 doi:10.1016/j.advwatres.2011.02.015, 2011.

720 Huang, C. S., Tsou, P. R., and Yeh, H. D.: An analytical solution for a radial collector well  
721 near a stream with a low-permeability streambed, *J. Hydrol.*, 446, 48–58,  
722 doi:10.1016/j.jhydrol.2012.04.028, 2012.

723 Huang, C. S., Lin, W. S., and Yeh, H. D.: Stream filtration induced by pumping in a confined,  
724 unconfined or leaky aquifer bounded by two parallel streams or by a stream and an  
725 impervious stratum, *J. Hydrol.*, 513, 28–44, doi:10.1016/j.jhydrol.2014.03.039, 2014.

726 Hunt, B.: Unsteady stream depletion from ground water pumping, *Ground Water*, 37(1),  
727 98–102, doi:10.1111/j.1745-6584.1999.tb00962.x, 1999.

728 Hunt, B.: Flow to vertical and nonvertical wells in leaky aquifers, *J. Hydrol. Eng.*, 10(6),  
729 477–484, doi:10.1061/(ASCE)1084-0699(2005)10:6(477), 2005.

730 Jasperse, J.: Planning, design and operations of collector 6, Sonoma County Water Agency,  
731 NATO Sci. Peace Secur., 169–202, doi:10.1007/978-94-007-0026-0\_11, 2009.

732 Kawecki, M. W.: Transient flow to a horizontal water well, *Ground Water*, 38(6), 842–850,  
733 doi:10.1111/j.1745-6584.2000.tb00682.x, 2000.

734 Kawecki, M. W. and Al-Subaikhy, H. N.: Unconfined linear flow to a horizontal well, *Ground*  
735 *Water*, 43(4), 606–610, doi:10.1111/j.1745-6584.2005.0059.x, 2005.

736 Kompani-Zare, M., Zhan, H., and Samani, N.: Analytical study of capture zone of a horizontal  
737 well in a confined aquifer, *J. Hydrol.*, 307, 48–59, doi:10.1016/j.jhydrol.2004.09.021,  
738 2005.

739 Kreyszig, E.: *Advanced engineering mathematics*, John Wiley & Sons, New York, 258, 1999.

740 Latinopoulos, P.: Analytical solutions for periodic well recharge in rectangular aquifers with  
741 third-kind boundary conditions, *J. Hydrol.*, 77(1), 293–306, 1985.

742 Lee, E., Hyun, Y., Lee, K. K., and Shin, J.: Hydraulic analysis of a radial collector well for  
743 riverbank filtration near Nakdong River, South Korea, *Hydrogeol. J.*, 20(3), 575–589,  
744 doi:10.1007/s10040-011-082-3, 2012.

745 Mohamed, A. and Rushton, K.: Horizontal wells in shallow aquifers: Field experiment and  
746 numerical model, *J. Hydrol.*, 329(1–2), 98–109, doi:10.1016/j.jhydrol.2006.02.006, 2006.

747 Neuman, S. P.: Theory of flow in unconfined aquifers considering delayed response of the  
748 water table, *Water Resour. Res.*, 8(4), 1031–1045, 1972.

749 Nyholm, T., Christensen, S., and Rasmussen, K. R.: Flow depletion in a small stream caused  
750 by ground water abstraction from wells, *Ground Water*, 40(4), 425–437, 2002.

751 Park, E. and Zhan, H. B.: Hydraulics of a finite-diameter horizontal well with wellbore storage  
752 and skin effect, *Adv. Water Resour.*, 25(4), 389–400, doi:10.1016/S0309-  
753 1708(02)00011-8, 2002.

754 Park, E. and Zhan, H. B.: Hydraulics of horizontal wells in fractured shallow aquifer systems,

755 J. Hydrol., 281(1–2), 147–158, doi:10.1016/S0022-1694(03)00206-3, 2003.

756 Rodriguez, L., Vives, L., and Gomez, A.: Conceptual and numerical modeling approach of the  
757 Guarani Aquifer System, Hydrol. Earth Syst. Sci., 17, 295–314, doi:10.5194/hess-17-295-  
758 2013, 2013.

759 Rushton, K. R. and Brassington, F. C.: Significance of hydraulic head gradients within  
760 horizontal wells in unconfined aquifers of limited saturated thickness, J. Hydrol., 492,  
761 281–289, doi:10.1016/j.jhydrol.2013.04.006, 2013a.

762 Rushton, K. R. and Brassington, F. C.: Hydraulic behavior and regional impact of a horizontal  
763 well in a shallow aquifer: example from the Sefton Coast, northwest England (UK),  
764 Hydrogeol. J., 21(5), 1117–1128, doi:10.1007/s10040-013-0985-0, 2013b.

765 Schafer, D. C.: Use of aquifer testing and groundwater modeling to evaluate aquifer/river  
766 hydraulics at Louisville Water Company, Louisville, Kentucky, USA, NATO Sci. Ser. IV  
767 Earth Environ. Sci., 60, 179–198, doi:10.1007/978-1-4020-3938-6\_8, 2006.

768 Steward, D. R.: Three-dimensional analysis of the capture of contaminated leachate by fully  
769 penetrating, partially penetrating, and horizontal wells, Water Resour. Res., 35(2),  
770 461–468, doi:10.1029/1998WR900022, 1999.

771 Su, G. W., Jasperse, J., Seymour, D., Constantz, J., and Zhou, Q.: Analysis of pumping-induced  
772 unsaturated regions beneath a perennial river, Water Resour. Res., 43(8), W08421,  
773 doi:10.1029/2006WR005389, 2007.

774 Sun, D. M. and Zhan, H. B.: Flow to a horizontal well in an aquitard-aquifer system, J. Hydrol.,  
775 321(1–4), 364–376, doi:10.1016/j.jhydrol.2005.08.008, 2006.

776 Sun, D. M. and Zhan, H. B.: Pumping induced depletion from two streams, Adv. Water Resour.,  
777 30, 1016–1026, doi:10.1016/j.advwatres.2006.09.001, 2007.

778 Todd, D. K. and Mays, L. W.: Groundwater hydrology, John Wiley & Sons, Inc., New Jersey,  
779 USA, 240, 2005.

780 Tsou, P. R., Feng, Z. Y., Yeh, H. D., and Huang, C. S.: Stream depletion rate with horizontal  
781 or slanted wells in confined aquifers near a stream, *Hydrol. Earth Syst. Sc.*, 14(8),  
782 1477–1485, doi:10.5194/hess-14-1477-2010, 2010.

783 Unland, N. P., Cartwright, I., Cendón, D. I., and Chisari, R.: Residence times and mixing of  
784 water in river banks: implications for recharge and groundwater–surface water exchange,  
785 *Hydrol. Earth Syst. Sc.*, 18, 5109–5124, doi:10.5194/hess-18-5109-2014, 2014.

786 Wang, C. T. and Yeh, H. D.: Obtaining the steady-state drawdown solutions of constant-head  
787 and constant-flux tests, *Hydrol. Process.*, 22(17), 3456–3461, doi:10.1002/hyp.6950,  
788 2008.

789 Yeh, H. D., Chang, Y. C., and Zlotnik, V. A.: Stream depletion rate and volume from  
790 groundwater pumping in wedge-shaped aquifers, *J. Hydrol.*, 349(3–4), 501–511,  
791 doi:10.1016/j.jhydrol.2007.11.025, 2008.

792 Yeh, H. D. and Chang, Y. C.: Recent advances in modeling of well hydraulics, *Adv. Water*  
793 *Resour.*, 51, 27–51, doi:10.1016/j.advwatres.2012.03.006, 2013.

794 Yeh, H. D., Huang, C. S., Chang, Y. C., and Jeng, D. S.: An analytical solution for tidal  
795 fluctuations in unconfined aquifers with a vertical beach, *Water Resour. Res.*, 46, W10535,  
796 doi:10.1029/2009WR008746, 2010.

797 Zhan, H. B. and Zlotnik, V. A.: Groundwater flow to a horizontal or slanted well in an  
798 unconfined aquifer, *Water Resour. Res.*, 38(7), doi:10.1029/2001WR000401, 2002.

799 Zhan, H. B. and Park, E.: Horizontal well hydraulics in leaky aquifers, *J. Hydrol.*, 281(1–2),  
800 129–146, doi:10.1016/S0022-1694(03)00205-1, 2003.

801 Zhan, H. B., Wang, L. V., and Park, E.: On the horizontal-well pumping tests in anisotropic  
802 confined aquifers, *J. Hydrol.*, 252(1–4), 37–50, doi:10.1016/S0022-1694(01)00453-X,  
803 2001.

804 Zheng, C. and Bennett, G. D.: *Applied contaminant transport modeling*, 2nd ed., Wiley-

805 Interscience, N.Y., 287, 2002.

806 Zhou, Y., Wenninger, J., Yang, Z., Yin, L., Huang, J., Hou, L., Wang, X., Zhang, D., and  
807 Uhlenbrook, S.: Groundwater–surface water interactions, vegetation dependencies and  
808 implications for water resources management in the semi-arid Hailiutu River catchment,  
809 China – a synthesis, *Hydrol. Earth Syst. Sci.*, 17, 2435–2447, doi:10.5194/hess-17-2435-  
810 2013, 2013.

811 Zlotnik, V. A.: A concept of maximum stream depletion rate for leaky aquifers in alluvial  
812 valleys, *Water Resour. Res.*, 40(6), W06507, doi:10.1029/2003WR002932, 2004.

813 **Table 1.** Symbols used in the text and their definitions.

Symbol	Definition
$a$	Shortest horizontal distance between stream 1 and the far end of lateral
$\bar{a}$	$a/y_0$
$b_1, b_2$	Thicknesses of streambeds 1 and 2, respectively
$d$	Shortest horizontal distance between the far end of lateral and location of having only horizontal flow
$\bar{d}$	$d/y_0$
$H$	Aquifer thickness
$h$	Hydraulic head
$\bar{h}$	$(K_y H h)/Q$
$K_x, K_y, K_z$	Aquifer hydraulic conductivities in $x$ , $y$ and $z$ directions, respectively
$(K_1, K_2)$	Hydraulic conductivities of streambeds 1 and 2, respectively
$L_k$	Length <del>from <math>x</math> axis to</del> $k$ -th lateral where $k \in (1, 2, \dots, N)$
$\bar{L}_k$	$L_k/y_0$
$N$	The number of laterals
$Q$	Pumping rate of point sink or radial collector well
$p$	Laplace parameter
$p_i$	$-\kappa_z \lambda_i^2 - \kappa_x \alpha_m^2 - \beta_n^2$
$p'_i$	$-\kappa_z \lambda_i^2 - \beta_n^2$
$p_0$	$\kappa_z \lambda_0^2 - \kappa_x \alpha_m^2 - \beta_n^2$
$p'_0$	$\kappa_z \lambda_0^2 - \beta_n^2$
$R$	Shortest horizontal distance between the far end of lateral and aquifer lateral boundary
$S_s, S_y$	Specific storage and specific yield, respectively
$t$	Time since pumping
$\bar{t}$	$(K_y t)/(S_s y_0^2)$
$w_x, w_y$	Aquifer widths in $x$ and $y$ directions, respectively
$\bar{w}_x, \bar{w}_y$	$w_x/y_0, w_y/y_0$
$X_n$	Equaling $X_{m,n}$ defined in Eq. (39) with $\alpha_m = 0$
$X_{n,k}$	Defined in Eq. (45)
$x, y, z$	Cartesian coordinate system
$\bar{x}, \bar{y}, \bar{z}$	$x/y_0, y/y_0, z/H$
$\bar{x}_k$	Coordinate $\bar{x}$ of the far end of the $k$ -th lateral

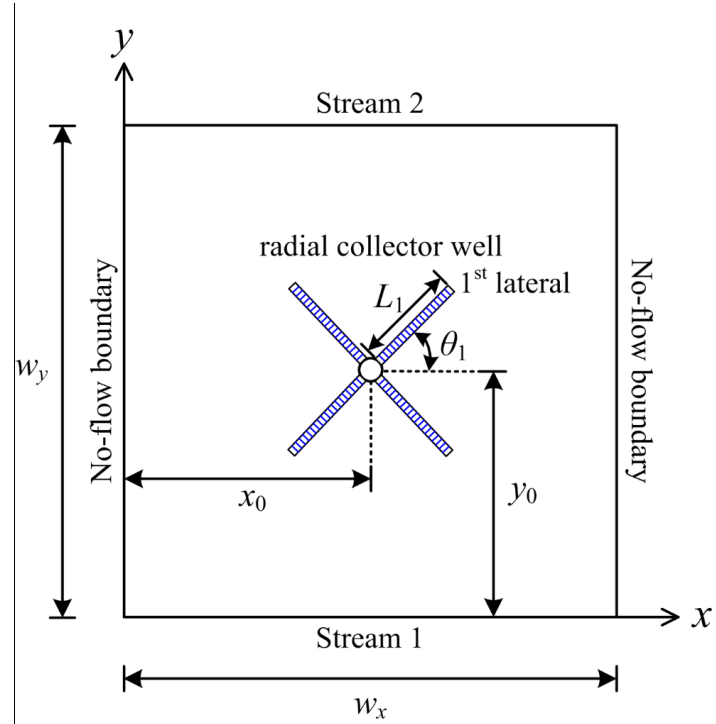


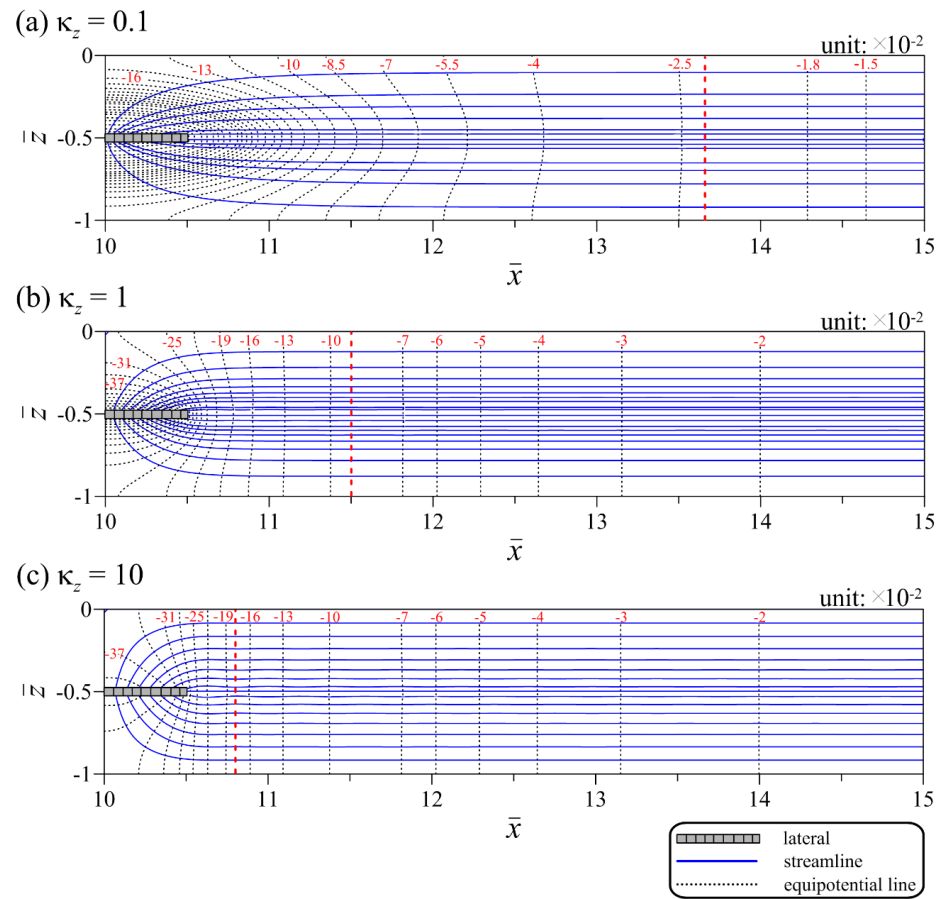
---

$x_0, y_0, z_0$	Location of center of RCW
$\bar{x}_0, \bar{y}_0, \bar{z}_0$	$x_0/y_0, 1, z_0/H$
$x'_0, y'_0, z'_0$	Location of point sink
$\bar{x}'_0, \bar{y}'_0, \bar{z}'_0$	$x'_0/y_0, y'_0/y_0, z'_0/H$
$\alpha_m$	$m \pi / \bar{w}_x$
$\beta_n$	Roots of Eq. (19)
$\phi_n$	Equaling $\phi_{m,n}$ defined in Eq. (32) with $\alpha_m = 0$
$\gamma$	$S_y / (S_s H)$
$\kappa_x, \kappa_z$	$K_x / K_y, (K_z y_0^2) / (K_y H^2)$
$\kappa_1, \kappa_2$	$(K_1 y_0) / (K_y b_1), (K_2 y_0) / (K_y b_2)$
$\lambda_0, \lambda_i$	Roots of Eqs. (40) and (41), respectively
$\lambda_s, \lambda'_s$	$\sqrt{(\kappa_x \alpha_m^2 + \beta_n^2) / \kappa_z}, \beta_n / \sqrt{\kappa_z}$
$\mu_{n,0}$	Equaling $\mu_{m,n,0}$ defined in Eq. (36) with $\alpha_m = 0$
$\nu_{n,i}$	Equaling $\nu_{m,n,i}$ defined in Eq. (37) with $\alpha_m = 0$
$\theta_k$	Counterclockwise angle from $x$ axis to $k$ -th lateral where $k \in (1, 2, \dots, N)$
$\max \bar{x}_k, \min \bar{x}_k$	Maximum and minimum of $\bar{x}_k$ , respectively, where $k \in (1, 2, \dots, N)$

---

## Figures





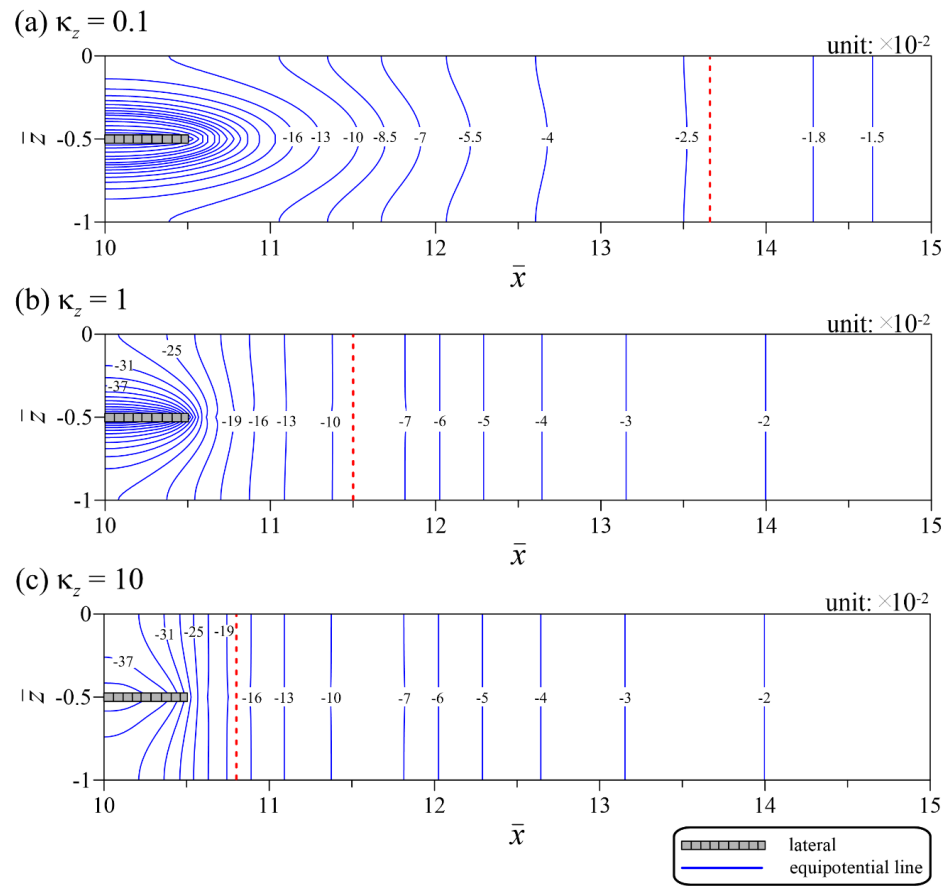
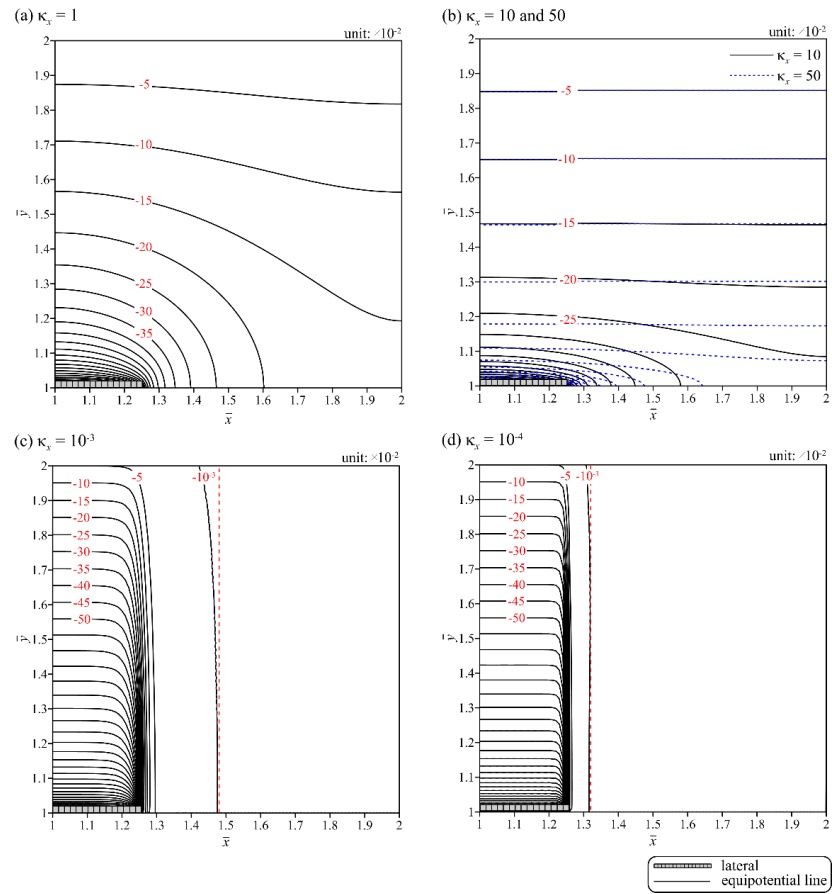
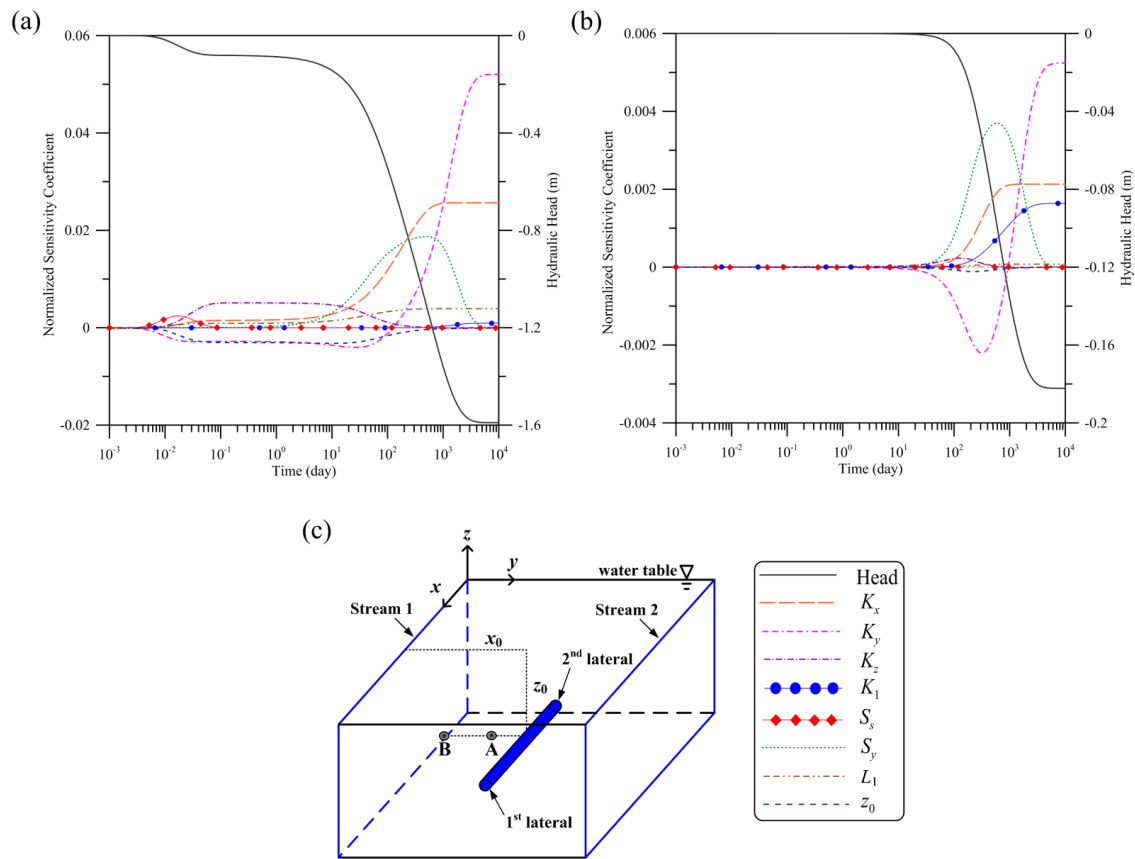


**Figure 2.** Streamlines and equipotential lines predicted by the present solution for  $\kappa_z =$  (a) 0.1, (b) 1 and (c) 10.



821

822 **Figure 3.** Spatial distributions of the dimensionless head predicted by the present head solution for  $\kappa_x =$  (a) 1, (b) 10 and 50, (c)  $10^{-3}$  and (d)  $10^{-4}$ .

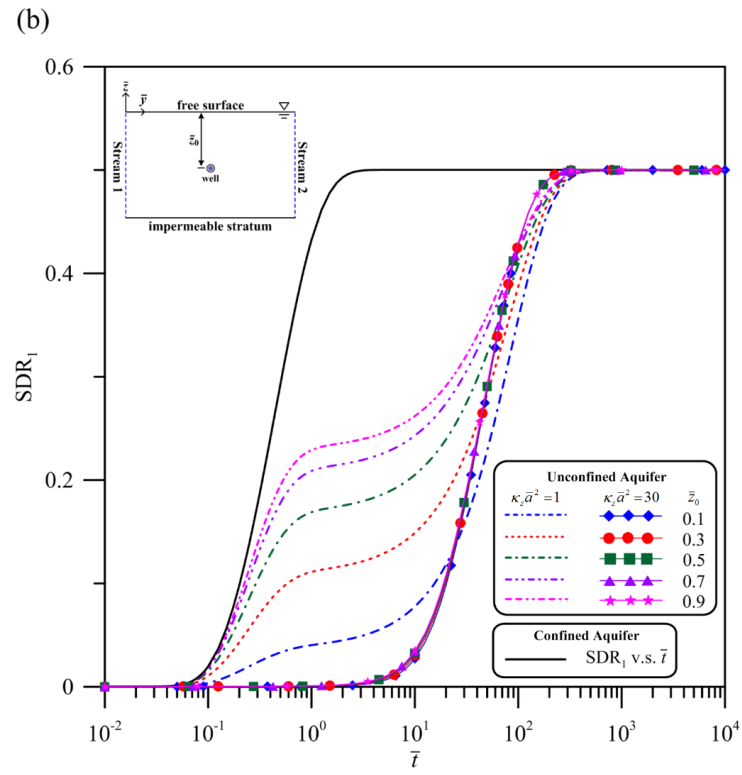
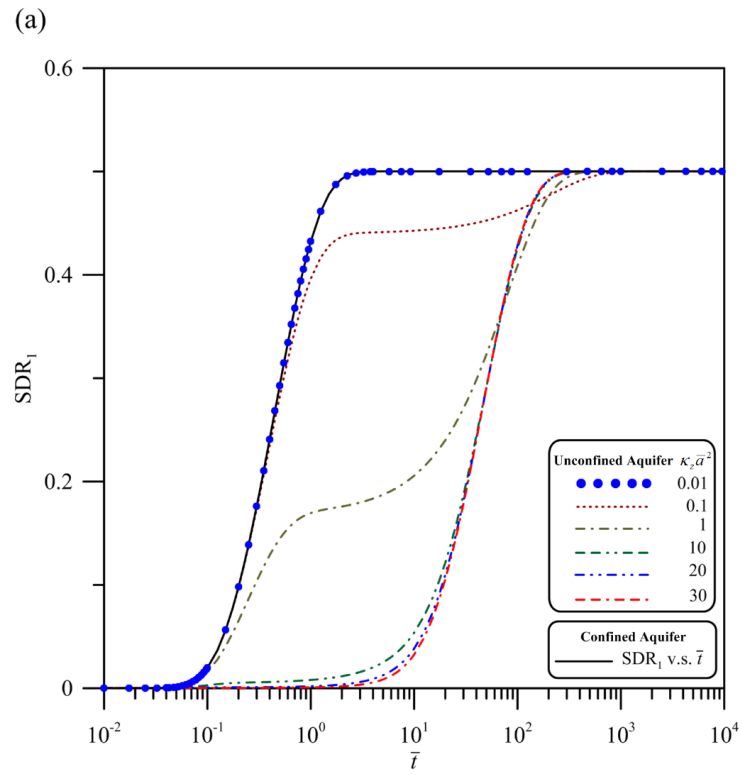


823

824

825

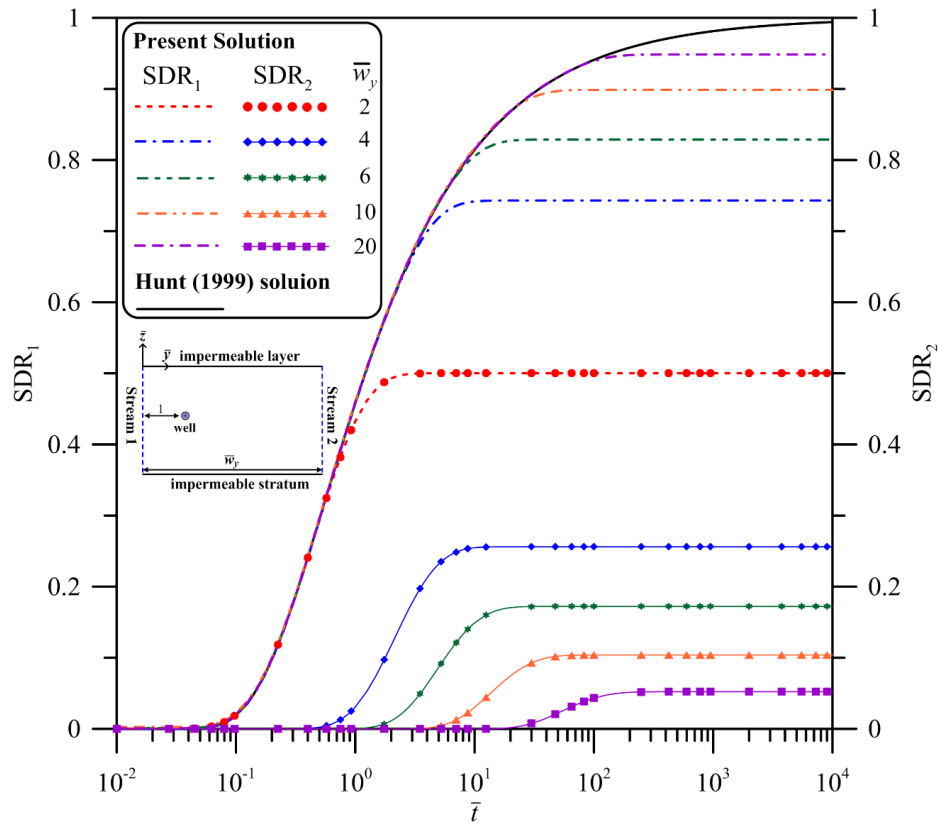
**Figure 4.** Temporal distribution curves of the normalized sensitivity coefficients for parameters  $K_x$ ,  $K_y$ ,  $K_z$ ,  $S_s$ ,  $S_y$ ,  $K_1$ ,  $L_1$  and  $z_0$  observed at piezometers (a) A of (400 m, 340 m, -10 m) and (b) B of (400 m, 80 m, -10 m).



826

827

**Figure 5.** Temporal SDR<sub>1</sub> distributions predicted by Eq. (52) for stream 1 with various values of (a)  $\kappa_z \bar{a}^2$  and (b)  $\bar{z}_0$ .



828

829 **Figure 6.** Temporal SDR distribution curves predicted by Eqs. (52) and (53) with  $\gamma = 0$  for confined aquifers when  $\bar{w}_y = 2, 4, 6, 10$  and  $20$ .